Master of Science Thesis

Heat Transfer Modification in a Particle-Laden Turbulent Channel Flow

For externally heated particles

Aviral Rajora

Friday 24th November, 2017

Faculty of Mechanical Engineering · Delft University of Technology

TU Delft Delft University of Technology

Challenge the future

Heat Transfer Modification in a Particle-Laden Turbulent Channel Flow

For externally heated particles

Master of Science Thesis

For obtaining the degree of Master of Science in Mechanical Engineering at Delft University of Technology

Aviral Rajora

Friday 24th November, 2017

Student number:	4518136	
P&E report number:	2863	
Thesis committee:	Dr. ir. Rene Pecnik,	TU Delft, supervisor
	Ir. Simone Silvestri,	TU Delft, Supervisor
	Prof. dr. D. J. E. M. Roekaerts,	TU Delft
	Dr. ir. W.- P. Breugem,	TU Delft
	Dr. ir. M. J. B. M. Pourquie,	TU Delft

An electronic version of this thesis is available at http://repository.tudelft.nl/.

Faculty of Mechanical Engineering · Delft University of Technology

Copyright © Aviral Rajora
All rights reserved.

Delft University Of Technology
Department Of
Process and Energy

The undersigned hereby certify that they have read and recommend to the Faculty of Mechanical Engineering for acceptance a thesis entitled **"Heat Transfer Modification in a Particle-Laden Turbulent Channel Flow"** by **Aviral Rajora** in partial fulfillment of the requirements for the degree of **Master of Science**.

Dated: Friday 24th November, 2017

Supervisor:

Dr. ir. Rene Pecnik

Supervisor:

Ir. Simone Silvestri

Abstract

Heat transfer in multiphase flows plays an important role in many industrial applications. For instance, particle-based solar receivers utilize the high absorptivity and heat capacity of dispersed phase in a carrier fluid to improve efficiency and heat transfer. This dispersed phase generally consists of a large number of small particles. It is, therefore, difficult to completely resolve such flows considering their finite size. Usually, these particles are so small, that they can be treated as point particles. This considerably reduces the computational effort, while preserving the essential characteristics of the particle-laden flows. In this thesis, the focus is on heat transfer modulation in a particle-laden turbulent channel flow using direct numerical simulations.

In flows with temperature gradients (for example, channel flow between hot and cold wall), particles absorb heat from hotter regions and release heat to colder regions, thereby enhancing heat transfer through particle feedback flux. On the other hand, presence of particles leads to decay in turbulence resulting in lower turbulent heat transfer. The interplay of this two phenomena can either increase or decrease the overall heat transfer based on Stokes number and thermal Stokes number (ratio of thermal response time to characteristic time scale of the flow).

To investigate the heat transfer modulation in particle-laden channel flow, the existing DNS code developed by Boersma [5] has been modified to include particle transport and heat transfer. The point-particle approach with two way coupling is implemented using trilinear interpolation scheme and 3^{rd} order Runge-Kutta time marching scheme. The implemented code is validated using the results from literature [20] for a flow with no external heating.

With the developed code, cases with no external source term and external source term with different optical thickness of the fluid have been analyzed. In order to focus only on the fluid-particle interaction, the effect of gravity is neglected and the flow is considered to be incompressible. It has been observed from these simulations that particles play an important role in modulation of heat transfer in such flows. Mean temperature profiles, heat flux mechanisms, temperature variance and budgets of temperature variance are studied extensively in order to understand the underlying phenomenon. It is found that the particle feedback heat transfer is the dominating mode in particle-laden flows.

Acknowledgements

This project required a large amount of research, work and dedication. However, it would have not been possible without the huge help of many individuals. First of all I would like to express my sincere gratitude to Dr. Ir. Rene Pecnik. I have been amazingly fortunate to have as my supervisor someone who demonstrated complete trust in me. He provided me with motivation, inspiration and independence to carry out my work. It is thanks to his availability and his willingness to dedicate me his time that I was able to develop and complete my master thesis project.

I also want to warmly thank Ir. Simone Silvestri for his kindness and willingness to help me during any hour of the day. I owe to his expertise the final form of this project. I am thankful to both for reading and reviewing extensively my report.

I would also like to acknowledge Ir. Ashish Patel for his time devoted in supervising me in the beginning of this work as well as for his valuable advises, and Ir. Hassan Nemati for his initial guidance.

I would also like to extend my gratitude to the teachers and students with whom I shared amazing experiences during my stint at TU Delft.

At last, most importantly, I express my deepest gratitude to my family, especially my parents for showering their love and support on me always. Their faith in me has been a constant source of inspiration for me.

Delft, The Netherlands
Friday 24th November, 2017

Aviral Rajora

Contents

List of Figures

List of Tables

Nomenclature

Latin Symbols

$\bar{q}_{mol}$	molecular heat flux
$\bar{q}_{part}$	particle feedback heat flux
$\bar{q}_{turb}$	turbulent heat flux
δ_v	viscous length scale
ϵ	viscous dissipation
ϵ_m	molecular dissipation term
η_k	Kolmogrov length scale
$\mathcal{P}_\theta$	turbulent production term
$\mathcal{Q}_{part}$	particle term
$\mathcal{T}_\theta$	turbulent transport term
μ_f	dynamic viscosity of fluid
ν_f	kinematic viscosity of fluid
ϕ_m	molecular diffusion term
ρ_f	density of fluid
ρ_f	density of particle
τ_f	characterstic time scale for fluid flow
τ_p	characterstic time scale for particle motion
τ_T	characterstic time scale for particle heat transfer
τ_w	wall shear stress
θ	non dimensional temperature
Bi	Biot number of particle

C_D	drag coefficient
$C_{p,f}$	specific heat capacity of fluid
$C_{p,p}$	specific heat capacity of particle
C_{pf}	specific heat capacity of fluid
d_p	diameter of particle
H	half channel width
h_f	heat transfer coefficient
I_{sun}	Sun's radiation intensity
k_f	thermal conductivity of fluid
k_p	thermal conductivity of particle
Nu	Nusselt number
Pl	Planck's number for the flow
Pr	Prandtl number
Q_r	radiation energy absorbed by particle per unit volume
Re_p	particle Reynolds number
Re_τ	friction Reynolds number
St_f	Stokes number for fluid flow
St_T	Stokes number for fluid heat transfer
u_τ	friction velocity

Chapter 1

Introduction

1.1 Motivation

Turbulent Flows

We observe turbulent flows in nature everyday, whether it be the water flowing down a river, the strong winds we experience, or we cycle on our way to work. Most of the fluid flow that we deal with in our everyday life are turbulent. When we wake up in the morning to make a cup of coffee, we have to thank turbulence for faster mixing of milk and coffee. When we move against the wind, we curse turbulence, for it is responsible for the aerodynamic drag we face. In short, turbulence can be a friend or foe in equal measure and we have to truly understand its true nature so that we can make it work to our advantage.

Despite being nearly ubiquitous, it is not easy to define turbulence. It is loosely defined based on some common characteristics, of which *randomness* or *chaotic* behaviour is the most common. A turbulent flow is characterized by random and chaotic three-dimensional motions of varying length and time scales. That means, no matter how carefully the boundary conditions are reproduced, the flow is never reproduced in detail. The second characteristic of turbulence is presence of '*vorticity*'. In fact, a strong three-dimensional vortex generation mechanism known as *vortex stretching* is believed to be responsible for transfer of energy from large scales to small scales, and hence being responsible for turbulence. The third important characteristic is that turbulence is strongly *diffusive* and *dissipative* in nature. Being 'dissipative' means that a turbulent flow quickly looses its kinetic energy and hence decays quickly(unless energy is not added to the flow). Perhaps, the best known intuitive characterization in this sense is presented by Richardson [37] in 1922:

Big whorls have little whorls,
which feed on their velocity;
And little whorls have lesser whorls,
And so on to viscosity.

This means that the mechanical energy is injected into a fluid at macroscopic scales, which is then cascaded down to microscopic scales until it is finally dissipated on molecular scales due to viscosity.

By 'diffusive' we mean that turbulent flows are very effective in mixing a fluid. In 1883, Osborne Reynolds [36] performed classic pipe flow experiment. He injected a dye stream into the centre of the pipe with flowing water and gradually increased the velocity of the flow. At low velocity, the dyed layer remained distinct throughout the length of the pipe. As the velocity was increased, the layer broke up and diffused across the cross section of the pipe. This is shown in figure 1.1. Figure 1.1a depicts laminar flow. Figure 1.1b is the case of turbulent flow. We observe enhanced mixing, which achieves the same result as that of molecular diffusion, but at an much faster time scale. Although, the end results of mixing is same as that of molecular diffusion, the physical mechanisms are completely different. Infact, turbulence arises when the molecular diffusion is actually very small compared to macroscopic transport. The ratio of these two quantities is a non dimensional parameter which Osborne Reynolds used for establishing the transition criteria from laminar to turbulent flow. It is called Reynolds number, and it can also be interpreted as the ratio of inertial forces to viscous forces. For a given flow configuration, there exists a critical Reynolds number, above which the flow becomes turbulent.

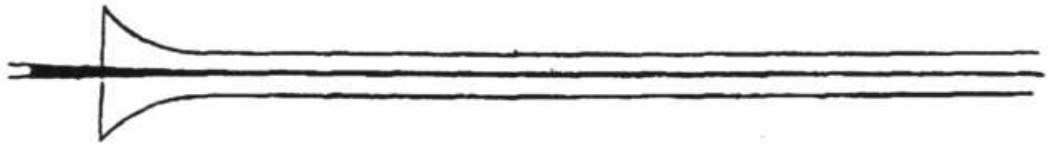

(a) Continuous streak of dye in laminar flow

(b) Mixing of dye in turbulent flow

Figure 1.1: Figure from Reynolds' 1883 [36] paper showing onset of turbulent flow

To summarize, there is no formal definition of turbulence, and often a formal definition is replaced by intuitive characterizations. A few important characteristics being the randomness or chaotic behaviour, large range of time and length scales, presence of strong vorticity, dissipativeness and enhanced diffusivity. A more mathematical characterization of turbulence would be in terms of high Reynolds Number, which means that inertial forces dominate the viscous forces.

Multiphase Flows

Multiphase flows, as evident from the name, are fluid flows consisting of more than one phase or component. Two general categories of multiphase flows can be identified easily, namely *dispersed flows* and *separated flows*. Separated flows are the ones in which two or more continuous streams of different fluids, separated by an interface, move together. Jet flows, slug flows in oil pipelines, etc. are some of the common examples of separated flows. Dispersed flows consists of finite particles, droplets or bubbles dispersed throughout the continuous phase of a liquid or a gas. Common examples of such flows include bubbles in soda, dust particles dispersed in air, etc.

Dispersed two-phase flows are encountered in numerous industrial and natural processes, for example, coal combustion, pneumatic conveying of particles, high heat capacity particles suspended in a liquid coolant, etc. Even the most elementary operations in processing technology, such as cavitating pumps and turbines, deal with multiphase flows. Incidentally, the ability to understand fluid flow behaviour is critical to the efficiency of such processes. Apart from industrial processes, mutiphase flows also find their place among critical biological and medical flows as well. Be it the oxygen transport through blood stream or niche surgical techniques like laser cavitation surgery, knowledge of multiphase flow behaviour is very important.

As evident, both turbulent and multiphase flows are widespread across nature and industries alike. Many a times, both these phenomena occur simultaneously and therefore, it is important to understand how they both interact with each other. This thesis is focussed on study of dispersed turbulent flows, as they find widespread industrial applications. Since both of these flows are very complex and non-linear in nature, mostly experimental or numerical techniques are employed to analyse them. A common numerical technique used is called Direct Numerical Simulations(DNS), where the smallest length and time scales are resolved. However, it should be noted that these techniques are computationally expensive and thus limits the scope of study to moderate Reynolds number flows. A more detailed discussion on the same is done in Chapter 3.

The interwining of phenomena in turbulent and multiphase flows results in interesting effects such as preferential concentration of moderate Stokes number particles, accumulation of particles in low speed streaks near the walls, turbophoresis, etc. Inspired by such interesting phenomena, this thesis focusses on how the heat released from irradiated particles plays a role in multiphase flows. Although, there has been an ongoing research for past few decades in turbulent multiphase flows, there are many interesting aspects that are not yet understood clearly. The main objective of this thesis is to explain heat transfer in a particle-laden channel flow when the particles in a optically thick medium receive heat from external source.

1.2 Objectives

The aim of the thesis can be divided into following broad categories:

- Identifying important non-dimensional parameters in studying turbulent multiphase flows with heat transfer.
- Carrying out literature survey to identify research gaps and to understand turbulent multiphase flows in more detail.
- Developing a Fortran code for Lagrangian tracking of dispersed phase and couple it with existing DNS code.
- Conducting Direct Numerical Simulations to investigate the effect of presence of particles on heat transfer in turbulent channel flow.
- Identifying important mechanisms to characterize heat transfer in particle-laden flows.

1.3 Outline

Chapter 2 presents a theoretical background. In this chapter, the governing equations are described and important non-dimensional parameters are identified. A short discussion on particle fluid behaviour and existing literature is also done in this chapter.

Chapter 3 discusses the modelling strategies used in this thesis. This chapter presents brief theory related to Direct Numerical Simulations and adopted methodology for particle-tracking. It also briefly highlights the coupling approach used for particle-fluid interaction.

Chapter 4 focusses on the numerics of the DNS code that is developed in this thesis. It starts with a short description of existing DNS code and subsequently discusses particle-tracking module. This involves discussion on interpolation techniques, implementation of coupling term and parallel implementation of the particle-tracking module.

Chapter 5 presents important and relevant results, pertaining to this study. This chapter also reasons possible mechanisms behind these results.

Chapter 6 summarises the finding of present work with recommendations of possible research direction.

Chapter 2

Theoretical Background

In engineering practices, like solar recievers, sediment transport, etc., fluid flows are often wall bounded and interact with particles. To discuss such flows, this chapter is divided into two main parts namely,

- *Turbulent Flows*
- *Particle-Laden Flows*

In the first section, the known theory on turbulent flows will be addressed. Since, the focus of this thesis is internal wall bounded channel flows, some characterstic effects occuring in channel flows will be emphasized. The section deals with both flow and heat transfer effects.

In the second section, the basic theory behind particle behaviour in a fluid is discussed. The section deals with particle motion and its thermal behaviour in a fluid.

2.1 Turbulent Flows

2.1.1 Basics of Fluid Flow

The fluid flow is described by conservation of mass, equation (2.1) and conservation of momentum, equation (2.2). The heat transfer in a fluid is governed by conservation of energy, equation (2.3) The gravity is neglected in present research and the flow is considered to be incompressible. The equations are

$$\frac{\partial u_i}{\partial x_i} = 0, \tag{2.1}$$

$$\rho_f \frac{\partial u_i}{\partial t} + \rho_f u_j \frac{\partial u_i}{\partial x_j} = -\frac{\partial p}{\partial x_i} + \mu_f \frac{\partial^2 u_i}{\partial x_j^2} + F_{2w}, \tag{2.2}$$

$$\rho_f C_{p,f} \frac{\partial T}{\partial t} + \rho_f C_{p,f} u_j \frac{\partial T}{\partial x_j} = k_f \frac{\partial^2 T}{\partial {x_j}^2} + Q_{2w}, \tag{2.3}$$

where, F_{2w} and Q_{2w} are the particle force and heat transfer due to particles on to the fluid per unit volume.

From a numerical point of view and to define non-dimensional groups, it is useful to make these equations non-dimensional. Non-dimensionalisation of equations gives rise to certain non-dimensional flow parameters such as Reynolds number, Prandtl number etc., which simplifies the characterization of the flows in general sense and makes the analysis more structured and simpler. In order to make the variables non-dimensional, they are scaled on constant values based on geometry or flow conditions. Non-dimensional variables are defined as

$$u^* = \frac{u}{u_\tau}, x^* = \frac{x}{H}, t^* = t\frac{u_\tau}{H}, \theta^* = \frac{T - T_c}{T_h - T_c} \tag{2.4}$$

where, u_τ is the friction velocity, H is the half channel width, T_c is the temperature of cold wall and T_h is the temperature of the hot wall.

Using these variables, the non-dimensional equations can be rewritten from equation (2.1), equation (2.2) and equation (2.3) as

$$\frac{\partial u_i^*}{\partial x_i^*} = 0, \tag{2.5}$$

$$\frac{\partial u_i^*}{\partial t^*} + u_j^* \frac{\partial u_i^*}{\partial x_j^*} = -\frac{\partial p*}{\partial x_i^*} + \frac{1}{Re_\tau} \frac{\partial^2 u_i^*}{\partial {x_j^*}^2} + f_{2w}^*, \tag{2.6}$$

$$\frac{\partial \theta^*}{\partial t^*} + u_j^* \frac{\partial \theta^*}{\partial x_j^*} = \frac{1}{Re_\tau Pr} \frac{\partial^2 \theta^*}{\partial {x_j^*}^2} + q_{2w}^*, \tag{2.7}$$

where, f_{2w}^* and q_{2w}^* are the non-dimensional feedback terms for momentum and energy transfer from the particle. These terms arise because of momentum transfer due to force on the particle and because of convective heat transfer between the fluid and particles. These terms are calculated as:

$$f_{2w}^* = \frac{\int_{\Omega^*} F_{2w}^p \delta(x - x_p) d\Omega^*}{\Omega^*} = \frac{\sum_{n=1}^{n_p} \left({F_{2w}^p}^* \delta(x - x_p) \right)}{\Omega^*} \tag{2.8}$$

and

$$q_{2w}^* = \frac{1}{Re_\tau Pr} \frac{\int_{\Omega^*} Q_{2w}^p \delta(x - x_p) d\Omega^*}{\Omega^*} = \frac{1}{Re_\tau Pr} \frac{\sum_{n=1}^{n_p} \left({Q_{2w}^p}^* \delta(x - x_p) \right)}{\Omega^*} \tag{2.9}$$

where,

$$F_{2w}^{p\ *} = -\frac{1}{2} C_D \left(\frac{\pi d_p^{*2}}{4} \right) (\vec{U_f^*} - \vec{U_p^*}) |\vec{U_f^*} - \vec{U_p^*}|, \tag{2.10}$$

$$Q_{2w}^{p\ *} = -\left(Nu\right) \pi d_p^* \left(\theta_f^* - \theta_p^*\right), \tag{2.11}$$

and Ω^* is the non-dimensional volume of the fluid element.

These terms are defined in detail in section (3.3) after a discussion on particle motion and thermal behaviour. For the current analysis of only the turbulent flows with no particles in this section these terms are zero, but will play a significant role when the analysis of particle-laden flows is considered later in this work.

The non dimensional parameters are then defined as:

- Reynolds number $Re = \frac{u_\tau h}{\nu}$ ratio of intertial and viscous forces.
- Prandtl number $Pr = \frac{\mu C_{p,f}}{\kappa}$ ratio of viscous diffusion rate and thermal diffusion rate.

From the non-dimensionalization of momentum equation, the flow can be characterized into two regimes:

- Laminar flow: Viscous terms dominate the inertial terms.
- Turbulent flow: Inertial terms dominate the viscous terms.

The pressure drop over the channel length is responsible for driving the flow. In a laminar flow, the disturbances are usually dampened out by the viscous forces. When the Reynolds number is high enough and a disturbance occurs, the viscous forces are unable to dampen out these disturbances and the flow becomes chaotic. This is called a turbulent flow. A turbulent flow is characterized by random velocity and pressure fluctuations and hence becomes unpredictable. Even though the exact flow is unpredictable, statistical flow variables can be obtained in time and space. These statistical values can be obtained using a procedure called Reynolds decomposition.

Reynolds Decomposition

The basic idea behind Reynolds decomposition is that the flow variable is separated in an average value (ensembled and spatial) and a deviation from that average value. Mathematically, this is decribed as:

$$u = \overline{U} + u', v = \overline{V} + v'.w' = \overline{W} + w', \theta = \overline{\theta} + \theta', p = \overline{P} + p', \tag{2.12}$$

where, $\bar{U}, \bar{V}, \bar{W}, \bar{\theta}, \bar{P}$ are the Reynolds' averaged values. The important thing to note is that when the values are decomposed in this manner, the average of fluctuating part has to be 0, which means,

$$\overline{u'} = 0, \overline{v'} = 0, \overline{w'} = 0, \overline{\theta'} = 0, \overline{p'} = 0. \tag{2.13}$$

To summarise, the following equation represents the mathematical relations between fluctuating and mean values

$$\overline{U}.\overline{W} = \overline{\overline{U}.\overline{W}}, \overline{U}.\overline{w'} = 0, \overline{u'}.\overline{W} = 0, \overline{u'w'} \neq 0. \tag{2.14}$$

By applying this Reynolds decomposition and averaging to the governing equations equation (2.5 -2.7) and dropping the * sign for brevity, we obtain the following non-dimensional equations for mean flow:

$$\frac{\partial \overline{u_i}}{\partial x_i} = 0, \tag{2.15}$$

$$\frac{\partial \overline{u_i}}{\partial t} + \overline{u_j}\frac{\partial \overline{u_i}}{\partial x_j} = -\frac{\partial \overline{p}}{\partial x_i} + \frac{1}{Re_\tau}\frac{\partial^2 \overline{u_i}}{\partial x_j^2} - \frac{\partial \overline{u_i' u_j'}}{\partial x_j}, \tag{2.16}$$

$$\frac{\partial \overline{\theta}}{\partial t} + \overline{u_j}\frac{\partial \overline{\theta}}{\partial x_j} = \frac{1}{Re_\tau Pr}\frac{\partial^2 \overline{\theta}}{\partial x_j^2} - \frac{\partial \overline{u_i' \theta'}}{\partial x_i}. \tag{2.17}$$

In equation (2.16), the term $\frac{\partial \overline{u_i' u_j'}}{\partial x_j}$ is what is called an unclosed term. This term can be interpreted as the transport of j component of fluctuating momentum per unit mass in i direction. It is similar to the momentum transfer of j component of mean flow per unit mass in i direction and has the same effect as the viscous stress between two layers. Therefore, it is also referred to as Reynolds stress.

Figure 2.1 shows measurements of stream-wise (w') and wall-normal velocity (u') components in a turbulent flow near a solid wall. It can be seen that u' and w' are correlated, yielding a negative Reynolds stress $\overline{u'w'}$; This suggests that there is a momentum transfer in which faster moving fluid is transported towards the wall and slower moving fluid away from the wall, i.e. a net transfer of momentum towards the wall that induces a (opposing) force on the plate. Similarily, the term $\overline{w'\theta'}$ can be interpreted as temperature transport.

2.1.2 Wall-bounded turbulent flows

The geometry of the channel used in this research is shown in figure 2.2. Coordinates x,y,z represent stream wise, span wise and wall normal directions respectively. The corresponding velocity components are u,v and w respectively. In previous section, variables u_τ and H were used for non-dimensionalization of the governing equation. In this section a closer look will be taken into the definition of these variables in the context of wall-bounded flows. Turbulent wall bounded flows are conventionally reported in terms of 'wall units', where the variables are non-dimensionalized using kinematic viscosity ν, the density ρ and the friction velocy u_τ of the fluid. The friction velocity, u_τ, depends on wall shear stress and is defined as:

$$u_\tau = \sqrt{\frac{\tau_w}{\rho}} \tag{2.18}$$

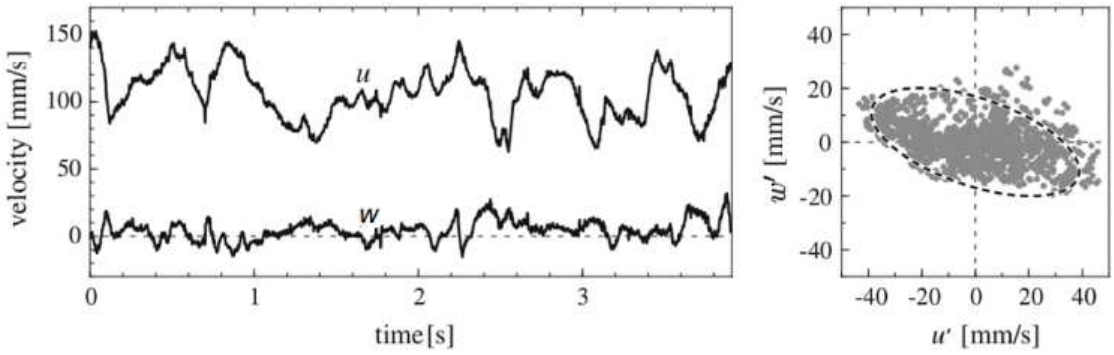

Figure 2.1: (*left*) Time series of measured stream-wise (u) and wall-normal (w) velocity components in a turbulent boundary layer over a flat plate at a distance of $z+ = 20$ viscous wall units. (*right*). The correlations of fluctuations, the ellipse represents the correlations between the two velocity components, i.e. $\overline{u'w'}$ called the *Reynolds Stress* (Data: A.D. Schwarz-van Manen). Figure taken from [28]

.

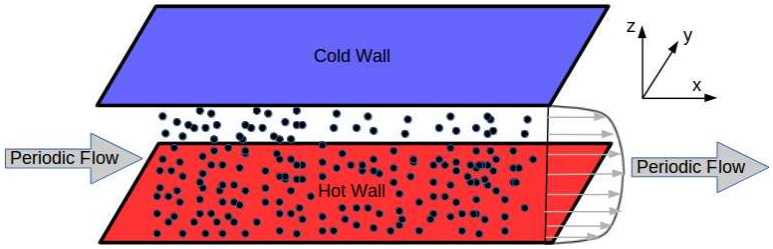

Figure 2.2: Geometry for Channel flow, wall-bounded in x-direction and periodic in y and z direction

where, τ_w is the wall shear stress.

Thus, it is to be noted that the friction velocity is infact a constructed variable used to define the momentum transfer at the wall by the wall shear stress.

Wall units are generally denoted by a '+' sign and therefore are also referred to as plus units. Important parameters non-dimensionalized into wall-units are length, time and velocity

$$z^+ = \frac{zu_\tau}{\nu}, t^+ = \frac{tu_\tau^2}{\nu}, u^+ = \frac{u}{u_\tau}. \tag{2.19}$$

By using this definition of z^+, a viscous lengthscale, δ_v can be defined using ν and u_τ as

$$\delta_v = \frac{\nu}{u_\tau}. \tag{2.20}$$

It is clear that reynolds number based on viscous length scale equals to unity and would be meaningless. Hence, instead of viscous length scale, *friction Reynolds number*, Re_τ is

defined based on half channel width as

$$Re_\tau = \frac{u_\tau H}{\nu}. \tag{2.21}$$

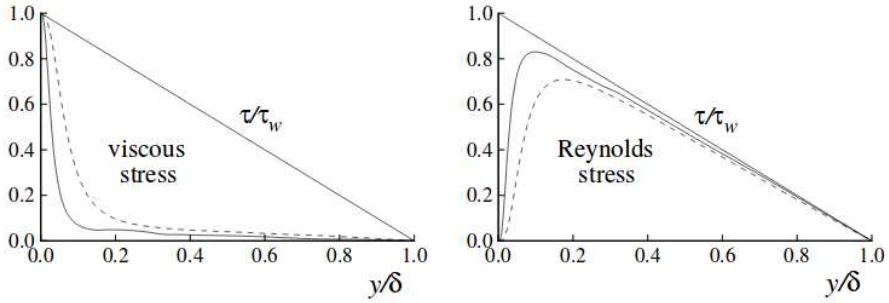

Figure 2.3: Profiles of the viscous shear stress, and the Reynolds shear stress in turbulent channel flow: DNS data of Kim et al.(1987) [18]. Figure legends : (- - -) Re = 5600; (——) Re = 13750

Figure 2.3 shows the balance between viscous and inertial stress in a turbulent wall bounded flow. It can be seen that near the wall, the viscous stress dominates while in the centre of the channel the reynolds stress dominates. This is expected as near the centre of channel, the flow behaves in a more turbulent manner.

Wall units can be used to make general rules for the structure of wall flows. Prandtl [34] in 1925, proposed the law of the wall, where he postulated that the flow near the wall is independent of channel height and the flow speed

$$\tau_w = \mu \frac{du}{dz} \approx \rho\nu \frac{u}{z} \Rightarrow \frac{\tau_w}{\rho} = \frac{\nu u}{z}. \tag{2.22}$$

If wall stress is written in the form of the friction velocity, equation (2.22) gives

$$\frac{\rho u_\tau^2}{\rho} = \frac{\nu u_\tau u^+}{\frac{\nu z^+}{u_\tau}} \Rightarrow u^+ = z^+. \tag{2.23}$$

The relation in equation (2.23) is consistent with the Prandtl's law of the wall. The region where this relation is valid is called the viscous sublayer which is approximately upto $z^+ = 5$. Above the viscous sublayer, lies the buffer layer where viscous and inertial effects roughly balance each other. This layer extends to around $z^+ = 30$ ([30]). Next is the overlap region, where logarithmic law of the wall holds as described in Pope [30]:

$$u^+ = \frac{1}{\kappa} ln z^+ + B \tag{2.24}$$

where κ and B are constants experimentally found to be approximately 0.41 and 5.2. The overlap extends to around $0.2H$. Above the overlap region is the outer layer, where influence of channel height and centreline velocity becomes important. To summarise, four layers are distinguished based on wall units, friction velocity, kinematic viscosity and channel height as follows:

- *Viscous sublayer* : $z^+ < 5$
- *Buffer layer* : $5 < z^+ < 30$
- *Overlap layer* : $30 < z^+ < 0.2H$
- *Outer layer* : $z^+ > 0.2H$

2.2 Particle-Laden Flows

In multiphase flows, many applications such as solar receivers, spray drying, sediment transport, etc. involve the turbulent flow as a carrier phase for particles or droplets entrained in the flow. Important parameters that influence the behaviour of such a mulptiphase flow system are ratio of density of particles to the density of flow, kinematic viscocity of the fluid and size of the diameter. The thermal behaviour is influenced by the above parameters along with heat capacity ratio of the particles and the fluid $\left(\frac{C_{p,p}}{C_{p,f}}\right)$ and thermal conductivity of the flow (k_f). In this section, the theory behind particle motion and thermal behaviour in a fluid is discussed.

2.2.1 Particle Motion

In this work, the particles are considered to be very small such that particle Reynolds number is small. For the linear motion of particles at very low Reynolds number, the particle motion is governed by the Basset-Boussinesq-Oseen(BBO) Equation ([41]). For a spherical particle, the BBO equation can be expressed as

$$\begin{aligned}\frac{\pi}{6}d_p^3\rho_p\frac{dU_p}{dt} = &\underbrace{\frac{1}{2}C_D\rho_f\left(\frac{\pi d_p^2}{4}\right)(U_f-U_p)|U_f-U_p|}_{\text{I}}\underbrace{-\frac{\pi}{6}d_p^3\nabla p}_{\text{II}}+\underbrace{\frac{\pi}{12}d_p^3\rho_f\frac{d}{dt}(U_f-U_p)}_{\text{III}}\\ &\underbrace{+\frac{3}{2}d_p^2\sqrt{\pi\rho_f\mu}\int_{t_0}^{t}\frac{\frac{d}{d\tau_p}(U_f-U_p)}{\sqrt{t-\tau_p}}d\tau_p}_{\text{IV}}+\underbrace{\sum_i f_i}_{\text{V}}\end{aligned} \tag{2.25}$$

where d/dt on the left hand side is the substantial derivative following the particle flow. The five terms on the right-hand side of the equation are:

- I : Force due to drag
- II : Force due to pressure gradient
- III : Force due to added mass effect
- IV : Force due to Basset history effect
- V : Extra body forces like gravitational force, electrostatic force etc.

Some authors also took into account the Faxen force for finite sized particles, but it has been shown by Homann[15] that these forces are significant only for larger particles, but negligible if particle diameter is equal or smaller than Kolmogrov length scale. The ratio of Faxen force to Stokes drag is given by,

$$\frac{F_{Faxen}}{F_{Stokes}} \approx \left(\frac{d_p}{l}\right)^2 \tag{2.26}$$

where l is the characterstic length scale for the fluid.

Thermophoresis is the physical phenomenon in which a temperature gradient in a gas causes suspended particles to migrate in the direction of decreasing temperature. A few authors include thermophoretic forces in there analysis, but such a force is significant only significant for flows in which the mean free path of the gas is slightly smaller than the size of the particle. As such, thermophoretic force is not taken into account in current analysis.

In the present work, body forces such as gravitational forces and electrostatic forces are neglected. For small heavy particles, Michaelides[27] has shown that the only significant force is the drag force, so equation (2.25) becomes

$$F_{fluid} = \frac{\pi}{6} d_p^3 \rho_p \frac{d\vec{U}_p}{dt} = \frac{1}{2} C_D \rho_f \left(\frac{\pi d_p^2}{4}\right) (\vec{U_f} - \vec{U_p})|\vec{U_f} - \vec{U_p}|, \tag{2.27}$$

where the subscripts 'f' and 'p' indicates fluid and particle parameters respectively. C_D is the drag force coefficient. There are many empirical relations available to calculate the drag force. The formulation of the drag coefficient C_D used here is the non-linear approximation given by Schiller and Naumann [40]

$$C_D = \frac{24}{Re_p}\left(1 + 0.15 Re_p^{0.687}\right), \tag{2.28}$$

where,

$$Re_p = \frac{d_p |U_f - U_p|}{\nu}. \tag{2.29}$$

Equation (2.27) can be rewritten in the form

$$\frac{d\vec{U_p}}{dt} = \frac{18\mu_f}{\rho_p d_p^2} \frac{C_D Re_p}{24} \left(\vec{U_f} - \vec{U_p}\right), \tag{2.30}$$

$$\frac{d\vec{U_p}}{dt} = \frac{\frac{C_D Re_p}{24}\left(\vec{U_f} - \vec{U_p}\right)}{\tau_p}, \tag{2.31}$$

where τ_p is called the particle relaxation time and is given by

$$\tau_p = \frac{\rho_p d_p^2}{18\mu_f}. \tag{2.32}$$

The particle relaxation time could be physically interpreted as the time which the particle takes to respond to motions of surrounding fluid. From equation (2.31), it can be seen that higher value of τ_p, means particle takes longer to adjust to changes in the surrounding fluid. A more accurate realization of this concept can be obtained, if the particle relaxation time is non-dimensionalized with the fluid characteristic time. The fluid characteristic time for a wall bounded flow is given by,

$$\tau_f = \frac{\mu_f}{\tau_w} = \frac{\nu}{u_\tau^2}. \tag{2.33}$$

The ratio of the particle relaxation time and fluid characterstic time is called Stokes number(St) and is given by,

$$St = \frac{\tau_p}{\tau_f}. \tag{2.34}$$

The Stokes number is an important parameter that it gives an idea as to what time scales of the flow, the particles can react significantly. A large Stokes number indicates that the changes in the fluid scales act in such a short span that particles can not completely adjust to the flow. That means, particles are not much affected by the faster changes in the flow. On the other hand, a low Stokes number indicates that the particles adjust quickly to the flow and hence can be considered as tracer particles.

2.2.2 Particle Thermal Behaviour

The thermal behaviour of particles is governed by the law of conservation of energy, and the governing balance equations are quite similar to the equations of motion of particle. The thermal balance equation is obtained by equating the increase in internal energy of particle to the net inflow of energy into the particle. In this work, particle receives external heat in the form of irradiation apart from inter-phase heat transfer from the fluid. For a particle in contact with the fluid, the inter-phase heat transfer rate between the particle and the flow is due to convective heat transfer and is given by

$$\dot{Q}_{conv} = (Nu)\pi d_p k_f (T_f - T_p). \tag{2.35}$$

where, Nu is the Nusselt number, k_f is the thermal conductivity of the fluid. The Nusselt number is calculated using the empirical relation given by the well know Ranz-Marshall correlation [35]

$$Nu = 2 + 0.6(Re_p)^{1/2}(Pr)^{1/3}. \tag{2.36}$$

The particle are also heated with an external radiation source. If Q_r is the radiation energy absorbed by the particle per unit volume, the total heat gained due to external source is given by

$$\dot{Q}_{rad} = \frac{Q_r \pi d_p^3}{6}. \tag{2.37}$$

Therefore, the total heat gained by the particle is given as

$$\dot{Q}_{tot} = \dot{Q}_{rad} + \dot{Q}_{conv} = (Nu)\pi d_p k_f (T_f - T_p) + \frac{Q_r \pi d_p^3}{6}. \tag{2.38}$$

If the particle diameter is small such that the Biot number (as defined in equation (2.39)) < 0.1, the temperature inside the particle can be considered to be uniform. Biot number is the ratio of convective heat transfer to conductive heat transfer.

$$Bi = \frac{h_f d_p}{k_p} \tag{2.39}$$

In present research, particle diameter is of the $\mathcal{O}(10^{-6})$. Therefore, the rate of increase in internal energy of particle is given as

$$\frac{dE}{dt} = \dot{m}_p C_{p,p} \frac{dT_p}{dt}. \tag{2.40}$$

where, $m_p = \frac{\pi d_p^3}{6}\rho_p$. Thus, from equation (2.38) and equation (2.40), the thermal balance equation for particle is obtained as

$$\frac{dE}{dt} = \dot{Q}_{tot} = \dot{Q}_{rad} + \dot{Q}_{conv}, \tag{2.41}$$

$$\frac{\pi d_p^3}{6}\rho_p C_{p,p} \frac{dT_p}{dt} = (Nu)\pi d_p k_f (T_f - T_p) + \frac{Q_r \pi d_p^3}{6}. \tag{2.42}$$

In order to define a parameter similar to the Stokes number, the balance equation is considered for a simple case with no radiation, such that particle energy source is due to convective heat transfer. The balance equation (2.42) then becomes,

$$\frac{\pi d_p^3}{6}\rho_p C_{p,p} \frac{dT_p}{dt} = (Nu)\pi d_p k_f (T_f - T_p). \tag{2.43}$$

Rearranging the terms, the above equation can be rewritten in the form,

$$\frac{dT_p}{dt} = (Nu)\frac{(T_f - T_p)}{2\tau_T} \tag{2.44}$$

where,

$$\tau_T = \frac{C_{p,p}\rho_p d_p^2}{12 k_f}. \tag{2.45}$$

τ_T is called the thermal response time. The thermal response time is analogous to the particle relaxation time defined in equation (2.32). It represents the time a particle needs to adapt to the temperature of the surrounding fluid. The thermal Stokes number can be

defined as the ratio of the thermal response time to the characteristic time scale of the fluid and is mathematically written as,

$$St_T = \frac{\tau_T}{\tau_f} \tag{2.46}$$

Equation (2.42) can be therefore written as:

$$\frac{\pi d_p^3}{6}\rho_p C_{p,p}\frac{dT_p}{dt} = \frac{\pi d_p^3}{6}\rho_p C_{p,p}(Nu)\frac{(T_f - T_p)}{2\tau_T} + \frac{Q_r \pi d_p^3}{6} \tag{2.47}$$

The above equation in non-dimensional form is written as

$$\frac{\pi d_p^{*3}}{6}\frac{d\theta_p^*}{dt^*}\frac{\rho_p C_{p,p}\Delta T u_\tau h^3}{h} = \frac{\pi d_p^{*3}}{6}(Nu)\frac{(\theta_f - \theta_p)}{2\tau_T^*}\frac{\rho_p C_{p,p}\Delta T u_\tau h^3}{h} + \left(\frac{Q_r^* I_{sun}}{h}\right)\frac{\pi d_p^{*3}}{6}h^3. \tag{2.48}$$

where Q_r is non-dimensionalized with $\frac{I_{sun}}{h}$. I_{sun} is the sun's radiation intensity.

In order to identify non-dimensional parameters, equation (2.48) is rearranged as,

$$\frac{d\theta_p^*}{dt^*} = (Nu)\frac{(\theta_f - \theta_p)}{2\tau_T^*} + Q_r^*\frac{I_{sun}}{\rho_p C_{p,p} u_\tau \Delta T} \tag{2.49}$$

or,

$$\frac{d\theta_p^*}{dt^*} = (Nu)\frac{(\theta_f - \theta_p)}{2\tau_T^*} + Q_r^*\frac{I_{sun}h}{k_f \Delta T}\frac{1}{Re_\tau Pr_p \frac{\rho_p}{\rho_f}} \tag{2.50}$$

or,

$$\frac{d\theta_p^*}{dt^*} = (Nu)\frac{(\theta_f - \theta_p)}{2\tau_T^*} + \frac{Q_r^*}{Re_\tau Pr_p Pl \frac{\rho_p}{\rho_f}}. \tag{2.51}$$

where, $Pr_p = \frac{C_{p,p}\mu_f}{k_f}$ and $Pl = \frac{k_f \Delta T}{I_{sun}h}$ is the Planck's number based on sun's radiation intensity, channel height and temperature difference between the two plates. It is the ratio of conductive heat transfer to radiative heat transfer due to external source.

2.3 Statistical behaviour of particles

In the previous section, equations of motion and energy for single particle were addressed. In this section, the overall behaviour of large number of particles will be discussed. The phenomena discussed with respect to particle motion are turbophoresis and preferential concentration.

2.3.1 Turbophoresis

In order to understand this phenomenon, it is useful to consider the two-fluid model. The basic assumption of the two-fluid model is to regard the group of dispersed particles as a continuous medium with continuous properties. The Reynolds averaged two fluid approach gives the particle momentum equation as [46]:

$$\frac{\partial(\alpha_2\rho_2\overline{U_{2i}})}{\partial t} + \frac{\partial(\alpha_2\rho_2\overline{U}_{2i}\overline{U}_{2j})}{\partial x_j} = -\frac{\partial(\alpha_2\rho_2\overline{u'_{2i}u'_{2j}})}{\partial x_j} + \overline{F_i}, \tag{2.52}$$

where α denotes the volume fraction and subscript 2 denotes the particle phase. This equation also assumes that the particles has same characteristics and properties throughout the domain. $\overline{F_i}$ is the force acting on the particles due to fluid.

Consider a situation in a particular direction, where there is no gradient of average fluid velocity (e.g. wall normal direction), the above equation (2.52) becomes,

$$\frac{\partial(\alpha_2\rho_2\overline{u'_{2i}u'_{2j}})}{\partial x_j} = \overline{F_i} \tag{2.53}$$

Equation (2.53) can be interpreted in the manner that the average drag force acting on the particles is balanced by the derivative of particle Reynolds stress and acts in the direction of declining Reynolds stress. This phenomenon where the particles have a tendency to move out of regions of lower fluctuations is termed as turbophoresis.

2.3.2 Preferential concentration

Preferential concentration as defined by Eaton et al. [10] is a mechanism which is driven by centrifuging of particles away from vortex cores and the accumulation of particles in convergence zones. This is represented in a simple manner in figure 2.4. Figure 2.4a shows that a particle moving around a two-dimensional vortex cannot follow the curved streamlines and moves away from its center. This effect is largely dependent on Stokes number of the particle. For a high Stokes number, particles will be ejected out of curving streamlines of the vortex due to higher inertia and will tend to be on the edges of the vortices and hence accumulate in converging flow regions. But the particles with very high inertia (or Stokes number) will have the tendency to move through vortices without much change in their velocity. Hence, in such cases the particles will not tend to "preferentially concentrate" on the edges of the vortices. Figure 2.4b shows a converging flow, characterized by high strain rate and low vorticity. As described previously, we observe a particle crossing the curved streamlines. In this case, a high concentration is expected in the central region.

2.4 Previous study : passive heat transfer in particle-laden turbulent channel flow

The main objective of this thesis thesis is to study heat transfer in a turbulent particle-laden channel flow. Several DNS studies have been conducted to study turbulent heat

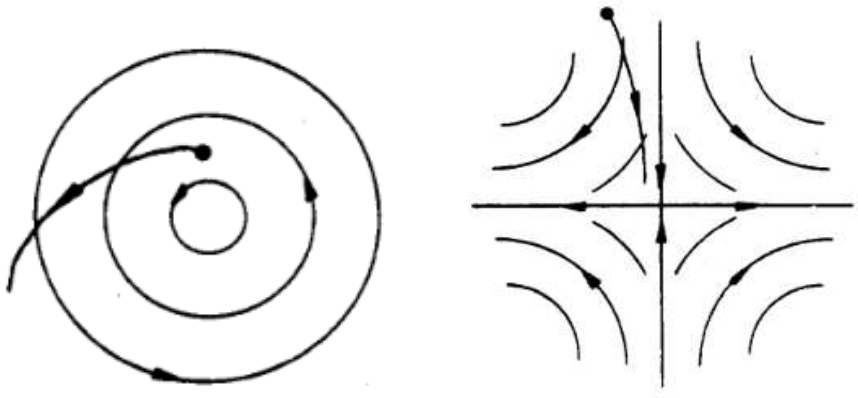

(a) In the neighbourhood of vortex

(b) In a converging flow

Figure 2.4: Particle interaction in simple two-dimensional flows

transfer in wall bounded flows. Although a significant amount of research has been done for particle-laden turbulent channel flow, heat transfer in such flows is still a very important aspect that has not been completely understood. A very systematic analyses of Reynolds number and Prandtl number as well as of mass loading and inertia has been performed by Kasagi [17] and Lyons et al. [22]. The modulation of heat transfer due to fluid-particle interactions can be important at even low mass loadings [16]. Zonta et al. [51] observed an increase in heat transfer flux at the walls for smaller particles and decrease in the same for larger particles. Poursani et al. [33] recently studied the effects of fluid heating by particles on turbulent evolution. They also showed that the pressure dilation term introduces turbulent kinetic energy at a range of scales consistent with the scales observed in particle clusters. However, they did this study for optically thin medium, such that the particles are heated uniformly through an external source. To the authors knowledge, there has been no study of heat transfer for externally heated particles in a optically thick fluid. That means the particles are not heated uniformly, but the external heat falling on the particles in the form of radiation is a function of optical thickness of the fluid. This thesis will focus on important aspects of heat transfer in such cases where the particle receive heat from an external source in optically thin as well as optically thick medium.

Chapter 3

Modelling Strategies

3.1 Direct Numerical Simulation

Direct numerical simulations resolves the flow field entirely and hence do not need any closure models as in Reynolds Averaged Navier-Stokes (RANS) solvers. In order to resolve all the flow scales, the cell size should be as small as the smallest scales of the flow. The smallest sales of the flows are comparable to the Kolmogrov scales ([30]). The Kolmogrov length scales are defined as:

$$\eta_K \approx \left(\frac{\nu^3}{\epsilon}\right)^{1/4} \tag{3.1}$$

where, ν is the kinematic viscosity and ϵ is the viscous dissipation.

Thus, the maximum element size is $\Delta L = \eta_K$ and the number of required mesh points is $N = (L/\eta_K)^3$. Putting the value of η_K from equation (3.1), we get

$$N \approx Re^{9/4} \tag{3.2}$$

If $Pr > 1$ the required number of grid cells must be increased by a factor of $\sqrt{Pr}$ in order to resolve the smaller scales of thermal turbulence [4].

The time step size should also be smaller than the Kolmogrov time scales. Therefore, $dt \approx t_\eta$, where $t_\eta = (\nu/\epsilon)^{1/2}$.

The domain size must be large enough to capture and reproduce the large eddy behaviour. In case of particle laden flows, this requirement means that the domain size is at least equal to 70H [47]. However, Zonta et al. [51], Kuerten et al. [20] etc. have carried out DNS studies with much smaller domains. Such cases, although the flow is not completely uncorrelated, do provide a useful insight in terms of mean and fluctuations of velocity and temperature fields. The use of smaller domain size also leads to lesser computational effort without loss of important physics.

3.2 Modelling approaches in particle-laden flows

Particle-laden turbulent flows are universal. With the advances in computational efficiency of modern computers, it is possible to study these flows numerically in great detail. Based on the application, there are various numerical approaches that can be used. In this section, a few of these approaches are discussed.

3.2.1 Particle-resolved DNS

This is the most detailed method, in which the flow around each particle is completely resolved and the particle behaviour arises due to external forces and hydrodynamic forces from the surrounding fluid. Since the flow around each particle needs to be resolved, this approach requires computational grid which is smaller than the particle size. There exists many approaches for particle resolved direct numerical simulations. One of the methods involve body-fitted spherical grid around the particles, sometimes embedded in in a cartesian grid for the whole computational domain [23]. This method has been used for calculation of force in decaying homogeneous turbulence ([1],[7]) and recently for flow around an array of 64 fixed particle in isotropic turbulent flow by Vreman [49]. Immersed boundary method originally developed by Uhlmann [45] has been modified and used for simulating dense suspensions of neutrally buoyant spheres in a turbulent channel flow by Picano et al.[29]. Lattice Boltmann method has also been applied for simulating the particle-laden turbulent flows [8].

3.2.2 Lagrangian point-particle methods

Saffman[39] showed that the perturbation in the fluid due to presence of particle decays as the sum of two contributions, one as $\frac{1}{r}$ (long-range) and $\frac{1}{r^3}$ (short-range). If the particles are small compared to the length scale of the fluid and separated by a distance larger than particle diameter, only long range interactions are important [19]. Short-range interactions such as particle wakes can be justifiably neglected in cases when particle diameter are smaller than Kolmogrov length scales of the flow field. This effect is termed as point-particle assumption in the literature.

The particle-resolved DNS methods are restricted to small number of particles, which are not small compared to Kolmogrov scales. However, for application where millions of small particles need to be simulated, point-particle approach is very useful. This is the oldest type of Lagrangian simulation of turbulent flows [23]. Important quantities in this approach are Stokes number and thermal Stokes number. This approach has been used extensively in the past, with the earliest attempt incorporating only one-way coupling ([11],[26],[43]). Later works extended this approach to two-way coupled simulations ([31],[25]) and four-way coupled simulations that also takes into account particle-particle collisions ([50],[48]).

3.2.3 Eulerian methods

In this two fluid approach the particles are not considered individually, but by concentration and velocity fields ([9],[13]). This formulation requires extra set of momentum and energy equations for the particulate phase. The momentum and energy exchange is taken into account as source and sink. Such an approach is called an Euler-Euler approach. This approach can also handle polydispersity, if the governing Eulerian equations are derived consistently using the probabilty density function approach ([3]).

Figure 3.1 taken from paper from Balachandar [2] shows the plot of Stokes number $St = \frac{\tau_P}{\tau_k}$ versus nondimensional particle size. In the present work, the particle size $\left(\frac{d}{\eta}\right) \approx 0.5$ and Stokes number $St = 34.6$. From figure 3.1, it can be justifiably said that point-particle approach is an appropriate choice.

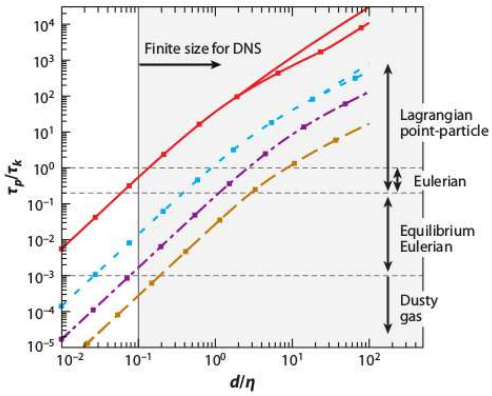

Figure 3.1: The plot of timescale ratio(τ_p/τ_κ) versus nondimensional particle size, for varying density ratio. The dashed gold line is for $\rho = 0$, the dashed-dotted purple line for $\rho = 2.5$, the dotted blue line for $\rho = 25$, and the solid red line for $\rho = 1000$. Figure taken from Balachandar [2]

3.3 Coupling approaches

An important consideration while modelling the particle-laden turbulent flows is the choice of coupling between the particles and the surrounding fluid.

The most common coupling approach for dilute flows is one-way coupling. Within the assumption of one-way coupling the particles experience force due to surrounding fluid, but the force or energy transfer due to particles onto the fluid is neglected. This is justified only if the particle concentration is very low i.e., below 10^{-5} [11]. DNS of particle laden flow using one-way coupling has been reported for various kinds of flows, e.g. pipe flows [32], homogeneous isotropic turbulence [42], etc. An extensive DNS study to benchmark particle statistics for one-way coupled channel flow has been carried out by Marchioli et al. [24].

While one-way coupling approach is applicable in dilute flows, for larger particle volume fractions the effect of particles on the fluid velocity and temperature can not be neglected and this reaction force or energy term needs to be taken into account. The non dimensional

governing equation for the fluid in this case takes the form of equation (2.6) and equation (2.7). Calculation of this force term is done by applying action-reaction principle to a generalized volume element, Ω containing a particle.

$$f_{2w} = \frac{\sum_{n=1}^{n_p} (F_{2w}^p)}{\Omega} \tag{3.3}$$

where,

$$F_{2w}^p = -F_{fluid} \tag{3.4}$$

and $F_{fluid} = \frac{1}{2} C_D \rho_f \left(\frac{\pi d_p^2}{4} \right) (\vec{U_f} - \vec{U_p}) |\vec{U_f} - \vec{U_p}|$ is defined in equation (2.27).

The non-dimensional feedback term,f_{2w}^* mentioned in equation (2.6) can be calculated as,

$$f_{2w}^* = \frac{f_{2w} \times h}{\rho_f u_\tau^2} = \frac{\sum_{n=1}^{n_p} \left({F_{2w}^p}^* \times \rho_f h^2 u_\tau^2 \right) h}{\Omega^* h^3 \rho_f u_\tau^2} \tag{3.5}$$

$$f_{2w}^* = \frac{\sum_{n=1}^{n_p} \left({F_{2w}^p}^* \right)}{\Omega^*} \tag{3.6}$$

where, ${F_{2w}^p}^* = -\frac{1}{2} C_D \left(\frac{\pi d_p^{*2}}{4} \right) (\vec{U_f^*} - \vec{U_p^*}) |\vec{U_f^*} - \vec{U_p^*}|$. Similarily, coupling term for energy equation can be calculated as:

$$q_{2w} = \frac{\sum_{n=1}^{n_p} (Q_{2w}^p)}{\Omega} \tag{3.7}$$

where,

$$Q_{2w}^p = -\dot{Q}_{conv} \tag{3.8}$$

and $\dot{Q}_{conv} = (Nu) \pi d_p k_f (T_f - T_p)$ is defined in equation (2.35).

The non-dimensional feedback term,q_{2w}^* mentioned in equation (2.7) can be calculated as,

$$q_{2w}^* = \frac{q_{2w} \times h}{\rho_f C_{p,f} u_\tau \Delta T} = \frac{\sum_{n=1}^{n_p} \left({Q_{2w}^p}^* \times k_f h \Delta T \right) h}{\Omega^* h^3 \rho_f C_{p,f} u_\tau \Delta T} \tag{3.9}$$

$$q_{2w}^* = \frac{\sum_{n=1}^{n_p} \left({Q_{2w}^p}^* \right)}{\Omega^*} \frac{k_f}{\rho_f C_{p,f} u_\tau h} = \frac{1}{Re_\tau Pr} \frac{\sum_{n=1}^{n_p} \left({Q_{2w}^p}^* \right)}{\Omega^*} \tag{3.10}$$

where, ${Q_{2w}^p}^* = -Nu \pi d_p^* \left(\theta_f^* - \theta_p^* \right)$.

In the above equations (3.3) and (3.7), n_p is the number of particles in the volume element, Ω. Since the governing equations are solved over the grid cell, the natural choice of Ω

is the volume of the grid cell. In order to calculate this force on the particle, there are two difficulties that must be dealt with. The first is that the calculation of drag force or convective energy transfer, the value of undisturbed fluid velocity and fluid temperature at the particle location should be known. If the effect of particles is taken into account, these undisturbed veloity and temperature values are not directly known. Boivin et al. [6] addressed this issues and concluded that the difference between the disturbed and undisturbed velocity is small if the particle diameter is small compared to grid size. Since in the point particle approach, it is assumed that the particle diameter is smaller than the Kolmogrov scale and in DNS grid size is of the order of Kolmogrov scale, this condition is somewhat satisfied.

The second difficulty is that the force exerted by the particles on to the fluid is discontinuous, which may cause numerical instabilities especially if the number of particles is small and the magnitude of particle force is large. Therefore, unless the particle concentration is too large, the force is distributed over a number of neighbouring grid points. However, if the number of particles is large enough, one could simply allocate the force to the grid cell in which the particle is located. The second approach is also used by Squires and Eaton [42].

For higher particle volume fraction, not only the effect of particle is important but the inter-particle interactions also become more and more important. Such a coupling which takes into account the force due to collisions is called the four-way coupling. Such simulations require additional algorithm to search for collisions and predict the outcome of such collisions. One of the such DNS study has been done by Sundaram and Collins [44].

Elghobashi [12] suggested the limits of validity of these coupling approaches for homogeneous isotropic turbulence. In the present simulation, the fluid is taken as air having density, ρ_f 1.3 kg/m^3 and specific heat 1007 J/kg K. The particles have a non-dimensional diameter ($\frac{d_p}{H}$) of 5.998×10^{-3}, density, ρ_p 1000 kg/m^3 and specific heat capacity 4186 J/kg K. The total number of particles in the channel is 2×10^6. The non-dimensional These conditions represent the one taken by Kuerten et al. [20], which also serves as our validation case. This gives the particle volume fraction as 1.4×10^{-3}, Stokes number, $St_f = \tau_p/\tau_f$, equal to 34.6 and thermal Stokes number, $St_T = \tau_T/\tau_f$, of 151. This values fall under the limits of two-way coupling method as suggested by Elghobashi [12] (see figure 3.2).

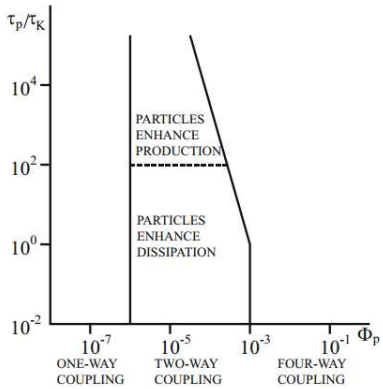

Figure 3.2: Map of regimes of interaction between particles and turbulence. Figure taken from Elghobashi [12]

Chapter 4

Numerical Details and Algorithms

This chapter is dedicated to explaining in short the numerical schemes and techniques that are used to study the particle laden turbulent flows. Before going into the details of particle tracking module that was essentially developed in this thesis, a brief discussion on the available DNS code developed by Boersma[5] is provided.

4.1 DNS Code for Fluid Flow

The study uses a cartesian code that discretises the spatial derivatives in wall-normal direction using a sixth order staggered compact finite difference scheme ([5]) and derivatives in homogeneous direction directions using a Fourier expansion with periodic boundary conditions. The equations are advanced in time using a third order Adams-Bashforth scheme, which provides good stability for both advection and diffusion terms [14]. A pressure correction scheme is used to correct the predicted velocity from Adams-Bashforth scheme, in order to ensure that the continuity equation is satisfied. This requires numerically solving of the Poisson equation. For the details of the algorithm, the reader is referred to Boersma[5].

4.2 Particle Tracking

The three main governing equation for particle motion and thermal behaviour as described in section (3.2) are:

$$\frac{\pi}{6} d_p^3 \rho_p \frac{d\vec{U}_p}{dt} = \frac{1}{2} C_D \rho_f \left(\frac{\pi d_p^2}{4} \right) (\vec{U_f} - \vec{U_p}) |\vec{U_f} - \vec{U_p}|, \tag{4.1}$$

$$\frac{d\vec{x}_p}{dt} = \vec{U_p}, \tag{4.2}$$

$$\frac{\pi d_p^3}{6}\rho_p C_{p,p}\frac{dT_p}{dt} = (Nu)\pi d_p k_f(T_f - T_p) + Q_r\frac{\pi d_p^3}{6}. \tag{4.3}$$

.

These equations can be rewritten in the form,

$$\frac{d\vec{U_p}}{dt} = \frac{3}{4}\frac{C_D}{d_p}\frac{\rho_f}{\rho_p}(\vec{U_f} - \vec{U_p})|\vec{U_f} - \vec{U_p}|, \tag{4.4}$$

$$\frac{d\vec{x_p}}{dt} = \vec{U_p}, \tag{4.5}$$

$$\frac{dT_p}{dt} = \frac{(Nu)\pi d_p k_f(T_f - T_p)}{\frac{\pi d_p^3}{6}\rho_p C_{p,p}} + \frac{Q_r}{\rho_p C_{p,p}}. \tag{4.6}$$

In order to solve these equations numerically, 3$^{\text{rd}}$ order explicit Runge Kutta scheme is employed in order to determine the updated velocity, location and temperature of the particle at the new time step. 3$^{\text{rd}}$ order Runge-Kutta method is a numerical method to approximate the solution of the initial value problem,

$$y'(x) = f(x, y); \qquad y(x_0) = y_0 \tag{4.7}$$

by evaluating the integrand f(x,y) three times per step. For step $n + 1$,

$$y_{n+1} = y_n + \frac{1}{6}(k_1 + 4k_2 + k_3) \tag{4.8}$$

where,

$$\begin{aligned} k_1 &= h(f(x_n, y_n), \\ k_2 &= hf(x_n + h/2, y_n + k_1/2), \\ k_3 &= hf(x_n + h, y_n - k_1 + 2k_2) \end{aligned} \tag{4.9}$$

and $x_n = x_0 + nh$.

4.3 Interpolation Schemes

In order to calculate the right hand side terms in equation (4.1) and equation (4.3), it is important to calculate the value of fluid velocity and fluid temperature at the location of the particle. However, the fluid velocities and temperature are known only at the centre (or faces in case of wall normal component) of the grid cells. Therefore, it becomes essential to interpolate these variables from cell centres (or cell faces) to the particle location. A number of algorithms are available to perform such an interpolation. Marchioli et al. [24] carried out a benchmarking of particle statistics in case of one-way

coupling and reports results from 5 research groups who used different interpolation techniques. The interpolation techniques used were 6^{th} order Lagrangian interploation, 4^{th} order Lagrangian interpolation, 3^{rd} order Hermite polynomial interpolation and Trilinear interpolation. The benchmarking test reports that the particle statistics do not differ significantly with the use of interpolation tecchniques. As such, the interpolation technique used in this work is the trilinear interpolation, which is second order accurate. The details of trilinear interploation are therefore discussed next.

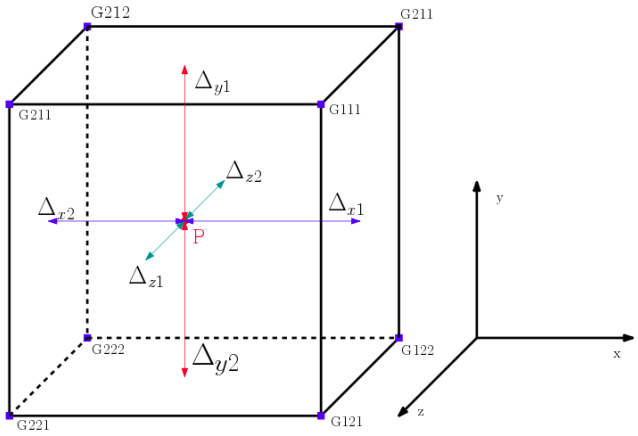

Figure 4.1: Depiction of trilinear interpolation

Figure 4.1 shows a situation in which fluid particle is located at the point P and the 8 surrounding grid cell centres are represented by the variable G111, G112, and so on. This kind of interpolation is similiar to bilinear interpolation in the sense that it is a fast and easy to implement algorithm. Suppose a quantity (say temperature, θ) is to be calculated at the location P of the particle, the interpolated value of the temperature θ is given by,

$$\begin{aligned}\theta_P =& \Delta X_1' \Delta Y_1' \Delta Z_1' \theta_{G111} + \Delta X_1' \Delta Y_1' \Delta Z_2' \theta_{G112} + \Delta X_1' \Delta Y_2' \Delta Z_1' \theta_{G121} \\ &+ \Delta X_1' \Delta Y_2' \Delta Z_2' \theta_{G122} + \Delta X_2' \Delta Y_1' \Delta Z_1' \theta_{G211} + \Delta X_2' \Delta Y_1' \Delta Z_2' \theta_{G212} \\ &+ \Delta X_2' \Delta Y_2' \Delta Z_1' \theta_{G221} + \Delta X_2' \Delta Y_2' \Delta Z_2' \theta_{G222}\end{aligned} \tag{4.10}$$

where, the variables $\Delta X_1'$,$\Delta Y_1'$, etc. are weigthed values of distance of particle location from the grid centre, defined as

$$\begin{aligned}&\Delta X_1' = \frac{\Delta X_1}{\Delta X_1 + \Delta X_2} \quad \Delta X_2' = \frac{\Delta X_2}{\Delta X_1 + \Delta X_2} \quad \Delta Y_1' = \frac{\Delta Y_1}{\Delta Y_1 + \Delta Y_2} \\ &\Delta Y_2' = \frac{\Delta Y_2}{\Delta Y_1 + \Delta Y_2} \quad \Delta Z_1' = \frac{\Delta Z_1}{\Delta Z_1 + \Delta Z_2} \quad \Delta Z_2' = \frac{\Delta Z_2}{\Delta Z_1 + \Delta Z_2}\end{aligned} \tag{4.11}$$

It should be noted that while intepolating the wall normal component of the velocity, the values are first interpolated to cell centre from the cell faces and then trilinear interpolation is applied to retrieve the wall normal fluid velocity at the particle location.

4.4 Parallel implementation of particle module

4.4.1 Storage of particle information

Since we do not know the number of particles in a given core at a given time, the storage of particle data is fundamentally different from storage of mesh. The number of particles in a particular core may increase or decrease, so the particle information needs to be dynamically stored. An efficient way to do this is storing the particle data in the form of singly linked lists. It is a type of data structure in which each node in the list stores the content of the node and a pointer to the the next node in the list. The content of the node in this case is the information of the particle such as particle location, particle velocity, etc. In a linked list, particles are scattered through memory and there is no need to worry about continuous memory block. The number of list elements i.e., particles can be easily removed by breaking or joining the links. The use of linked list to store particle information is efficient as it is very easy to remove or add particle information in a particular core of the memory as soon as particle moves out or in the core. Figure 4.2 depicts the structure of linked list.

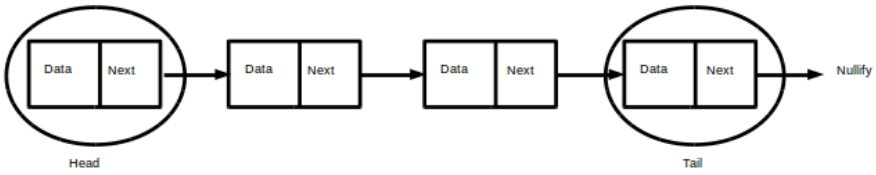

Figure 4.2: Depiction of singly linked list for storing particle information

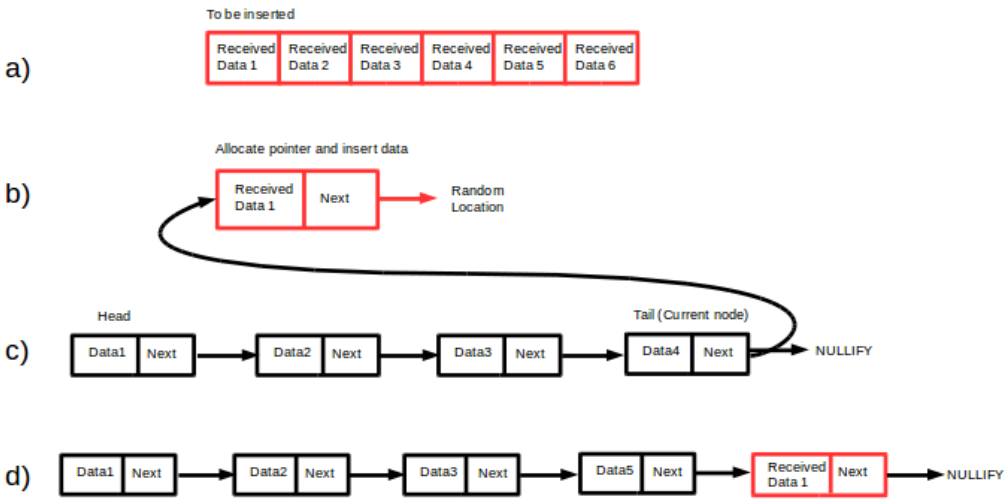

Figure 4.3: Depiction of insertion algorithm for particle linked list

Figure 4.4 shows the algorithm for removing a particle from the list. To delete a node from linked list, following steps are required:

- Find the particle node to be deleted (figure 4.4a).
- Store the particle information to be sent to the other core in an array (figure 4.4b).
- Link the next of previous node to the following node (figure 4.4c).
- Free memory for the node to be deleted using DEALLOCATE command (figure 4.4c).

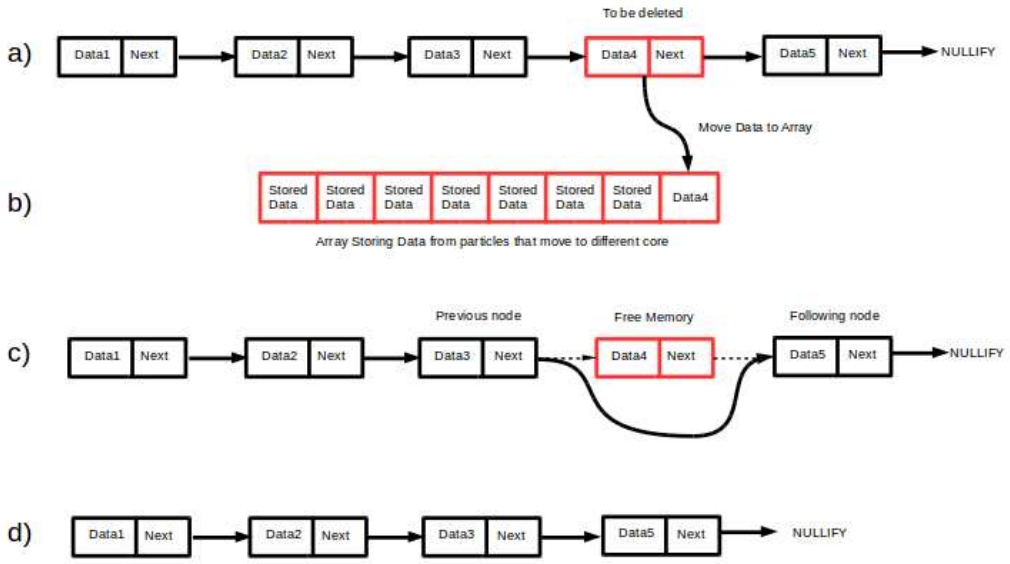

Figure 4.4: Depiction of deletion algorithm for particle linked list

Figure 4.3 shows the algorithm for adding the particle to the list. To insert a node to the end of linked list, following steps are required:

- Find the particle data to be inserted from the received array (figure 4.3a).
- Allocate memory for the new node using ALLOCATE command (figure 4.3b).
- Traverse to the end of the list to find the tail node (figure 4.3c).
- Link the current next link of tail node to point to new node (figure 4.3c).
- Update the tail link to the next link of new node (figure 4.3d).

4.4.2 Exchange of particle information between cores

The existing DNS code is parallelized in the spanwise and streamwise direction. A schematic representation of parallization with respect to channel flow is shown in figure 4.5. Each subdomain in solved independently in a particular core on the cluster, with information exchange between cores occuring through MPI (message passing interface). Particles moving in a turbulent flow constantly change their positions and move across cores. When a particle moves from one core to another the dynamic data occupied on

the old core has to be transfered to the new core. Since, the time step size is very small, the particle will move only to the neighbouring core as shown in figure 4.6. The particles moving from one core to another are stored in an array as described in section 4.4.1. This means that first different arrays are created for movement of particles to different cores. For example, if particles are to be sent from core 6 and core 8 to core 0 as shown in figure 4.6, first two arrays are created for movement from core 6-core 0 and core 8-core 0. These arrays are then sent from core 6 & core 8 to core 0 as shown in figure 4.6) to the neighbouring cores using *MPI_SEND*. These arrays are received by core 0 using *MPI_RECV* command. The linked lists of core 6 and core 0 are updated to remove the particle information from existing lists and the memory from the original cores is then freed using DEALLOCATE command. The particle information is added to the particle linked list of new core (core 0) using insertion algorithm as described in section 4.4.1. It is very critical to minimize the communication overhead in the MPI code, since the communication of data is between cores is a time consuming step. Therefore, this implementation, where all the data from corresponding cores is sent and received as an array of structure is efficient as it reduces the number of time consuming *MPI_SEND* and *MPI_RECEIVE* operations. Also, care has been taken to allocate the size of sending arrays dynamically to further reduce the time required in send and receive operations.

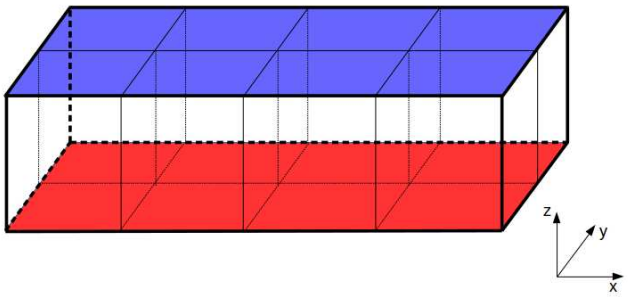

Figure 4.5: Parallelization of channel flow

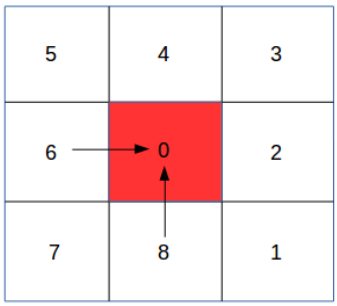

Figure 4.6: Depiction of movement of particles between cores

Chapter 5

Results and Discussions

5.1 Numerical Experiments

In this thesis, direct numerical simulations of fully developed particle-laden turbulent channel flow are performed. The main objective is to understand the modification in heat transfer when the particles receive heat from an external source. In order to study the effect of external source on heat transfer, we take four cases as described in table 5.1. These cases are chosen as to study the effect of optical thickness and thermal Stokes number on heat transfer modification.

Optical thickness can be understood as the ratio of geometric length scale to the radiative length scale. It is defined as

$$\tau = \int_0^H \kappa dz = \kappa H \tag{5.1}$$

where κ is the absorption coefficient (m^{-1}). $1/\kappa$ also denotes the radiative length scale over which the radiation is absorbed. A medium is called optically thick if $\tau > 1$ and optically thin if $\tau < 1$. A higher optical thickness means that the radiation energy is absorbed quickly in the channel over a short geometric length. The incoming incident radiation I varies along channel depth according to Beer-Lambert's law

$$I = I_0 e^{-\tau z}. \tag{5.2}$$

The absorbed energy density is given as

$$Q_r = \tau E_m - \tau G \tag{5.3}$$

Assuming, no emmision of energy through the fluid due to radiation, equation (5.3) becomes

$$Q_r = -\tau G \tag{5.4}$$

where, G is the incident radiation given by

$$G = \int_{\Omega} \frac{I}{4\pi} d\Omega. \tag{5.5}$$

Due to change in optical thickness, the variation of external radiation inside the channel differs significantly as shown in figures 5.1a and 5.1b. Case OT5 and case OT01 serve to study the variation in heat transfer due to optical thickness. Case OT01 correspond to optically thin medium, while cases OT5 and St50 correspond to optically thick medium. Case OT5 is compared with Case St50 to highlight the effect of thermal Stokes number. All these cases are compared with the base case of flow without the particles (Case NP). Case NH is also studied to focus on changes due to radiative heat received by the particles. All simulations are performed at fixed shear Reynolds number ($Re_\tau = 150$), constant density ratio ($\rho_p/\rho_f = 769.23$) and fixed number of particles ($N_p = 2 \times 10^6$) corresponding to volumetric fraction ($\phi_p \approx 1.4 \times 10^{-3}$). Each simulation is carried out with the concentration factor, $C_I = 60$ for normal solar intensity, $I_{sun} = 900.1215 W/m^2$. Therefore total intensity falling on the top wall of channel, $I_0 = C_I \times I_{sun}$. The temperature difference between the hot wall and cold wall ($T_h - T_c$) is set at $30K$. Gravity is neglected to isolate the effect of fluid-particle interaction. The half-channel width, H is kept constant at 1m. The Planck's number as defined in section (2.2.2) is the same for all cases and is calculated as:

$$Pl = \frac{k_f \Delta T}{I_{sun} H} = \frac{0.023 \times 30}{900.1215 \times 1} = 7.665 \times 10^{-4} \tag{5.6}$$

The domain size used in the simulations correspond to $2H \times 2\pi H \times 4\pi H$ in wall-normal, span-wise and stream-wise direction. The corresponding mesh size is $140 \times 140 \times 168$ and consists of 3,245,760 cells.

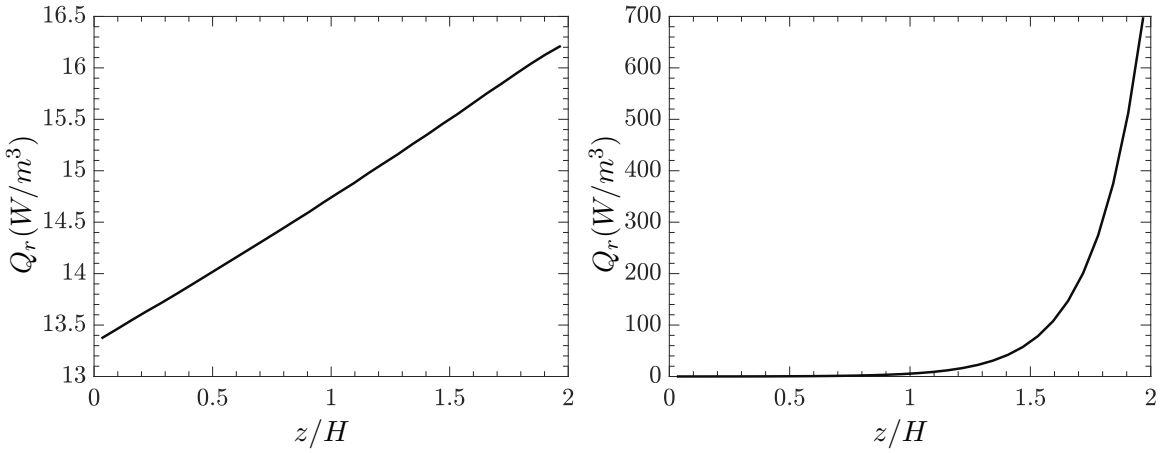

(a) Optical thickness = 0.1 (b) Optical thickness = 5

Figure 5.1: External heat source for different optical thickness

Case	$\frac{\rho_p}{\rho_f}$	Re_τ	Pr	N_p	St_k	St_T	*Optical thickness*
NP	-	150	0.71	-	-		-
NH	769.23	150	0.71	2×10^6	34.6	151	-
OT01	769.23	150	0.71	2×10^6	34.6	151	0.1
OT5	769.23	150	0.71	2×10^6	34.6	151	5
St50	769.23	150	0.71	2×10^6	34.6	50	5

Table 5.1: Simulation parameters for all cases

5.2 Validation of particle-laden DNS

While using a CFD code, it is important to validate the code to ensure reliability of results. This can be done by comparing the simulated case with a known result in similar setting. In present work, the case NH is compared with the results from Kuerten et al.[20]. Both present case NH and Kuerten et al. [20] use same simulation parameters, same interpolation scheme and empirical expressions for drag coefficient and Nusselt number. The difference between modelling strategies is that while the present work uses sixth order finite difference scheme, Kuerten et al. [20] use Chebyshev polynomials in wall-normal direction. Figures 5.2, 5.3 and 5.4 compare the present result with the results of Kuerten et al. [20] for mean stream-wise velocity, rms velocity and mean temperature for the fluid. As can be seen, all the three statistical quantities show reasonable agreement with the reported data in literature. The slight variation in the results may be attributed to the fact that Kuerten et al. [20] uses an extra smoothing of the source term (arising from two-way coupling) by distributing the contribution over eight neighbouring grid cells in order to make the particle tracking numerically more stable.

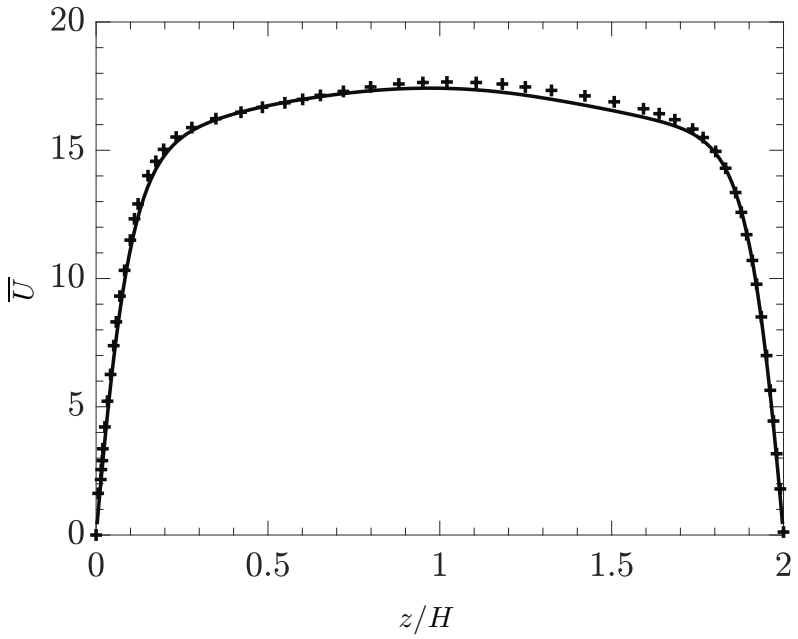

Figure 5.2: Mean streamwise fluid velocity as a function of wall-normal coordinate; Figure legends : (——) case NH, (✚ ✚ ✚) Kuerten et al. [20]

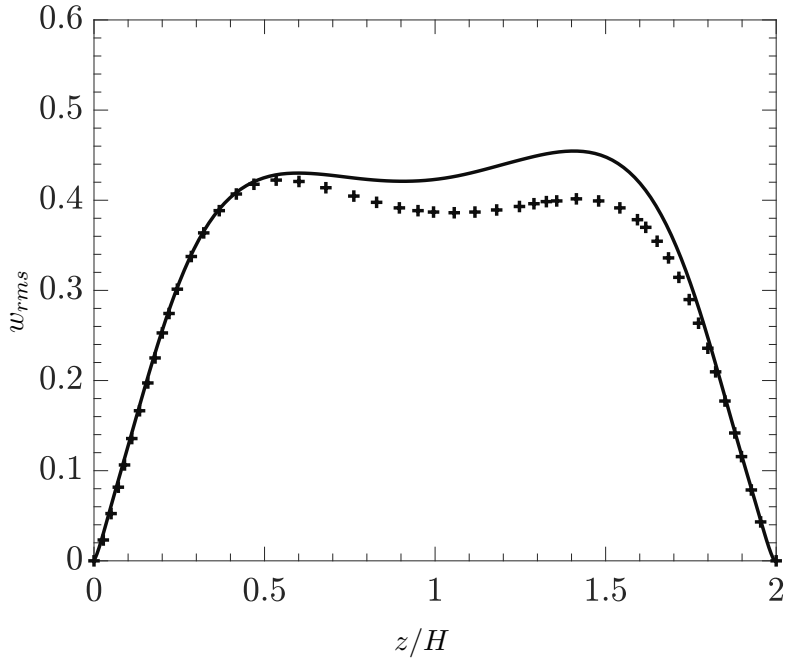

Figure 5.3: RMS of wall-normal component of fluid velocity as a function of wall-normal coordinate; Figure legends : (——) case NH, (✚ ✚ ✚) Kuerten et al. [20]

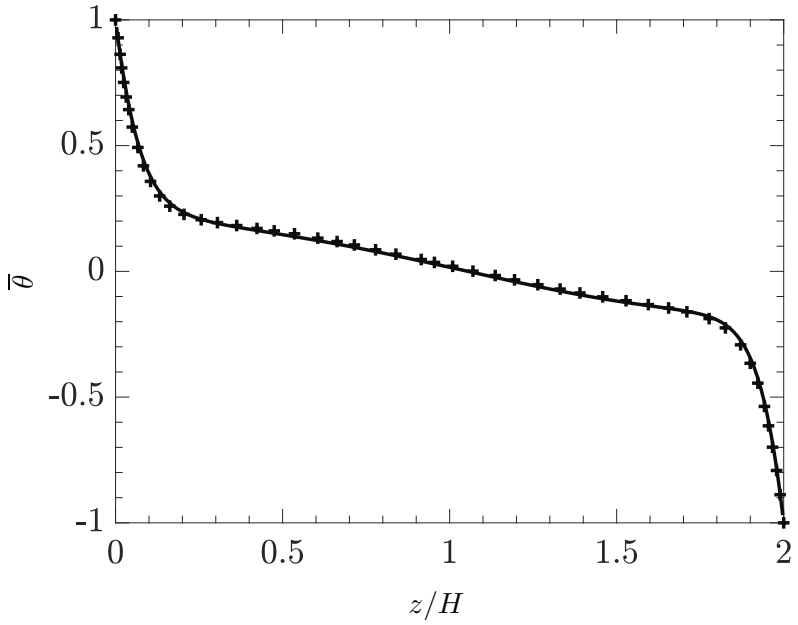

Figure 5.4: Mean fluid temperature as a function of wall-normal coordinate; Figure legends : (——) case NH, (✚ ✚ ✚) Kuerten et al. [20]

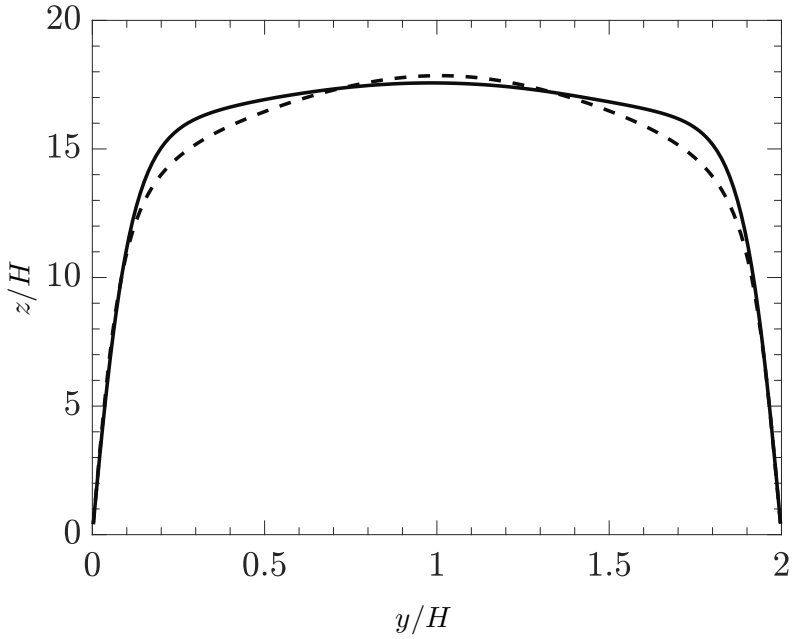

Figure 5.5: Mean streamwise velocity for case NH and reference case; Figure legends : (——) case NH, (– –) reference case

5.3 Fluid behaviour

In this section, a short discussion on the fluid behaviour in the presence of particles is provided. Since the Stokes number is kept constant for all the simulations, it is enough to focus on one case with the particles and compare it with the reference case. For the discussion, we consider the case NH.

The mean fluid velocity of the channel is increased compared to the reference case as can be seen in figure 5.5. The particle-laden flow tends increase bulk flow rate which is reflected in more turbulent profile of mean streamwise velocity in figure 5.5. Since the driving pressure gradient is the same, this enhanced mean velocity is equivalent with drag reduction [21]. This effect is also noted experimentally by Rossetti and Pfeffer [38] in 1972. Because of the effective increase in the bulk flow rate, the turbulent fluctuations are also altered. The streamwise velocity fluctuations are augmented and shifted slightly to the centre of the channel, while the spanwise and wall-normal velocity fluctuations reduces, along with substantial reduction in reynolds stress as can be seen in figure 5.6.

Figure 5.7 shows the mean values of drag force acting from the fluid on to the particles. The wall-normal drag component is slightly positive near the lower wall and slightly negative near the top wall but becomes vanishingly small in the core region. The mean Stokes force is therefore directed away from the wall and opposes the drift of particles towards the wall. This is known to be responsible for the tendency of inertial particles to accumulate in the near-wall regions as shown in figure 5.8 and figure 5.9. It can also be seen from figure 5.8 that the particles concentrate in the low speed streaks. It can be seen that the streamwise component of the drag is negative for the buffer layer and is positive for $Z+ > 30$. This means that in the buffer layer mean particle velocity exceeds the mean

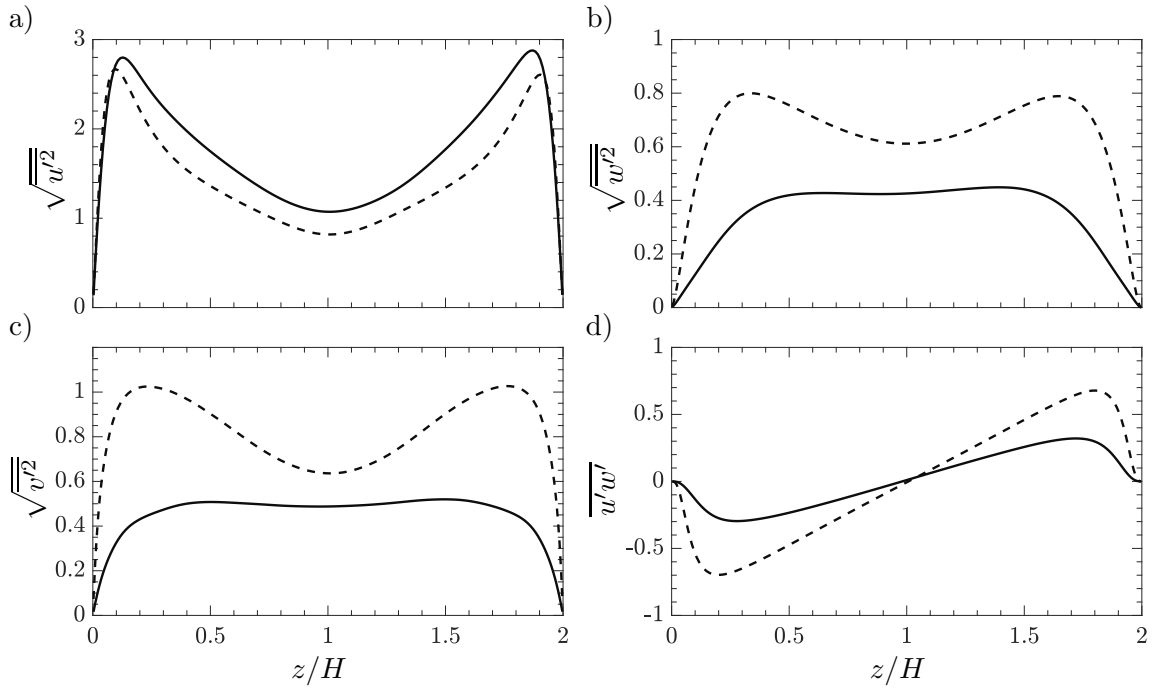

Figure 5.6: Statistics of fluid flow (a): RMS of streamwise velocity component; (b): RMS of wall-normal velocity component; (c):RMS of spanwise velocity component; (d): Reynolds Stress; Figure legends : (——) case NH, (– –) reference case

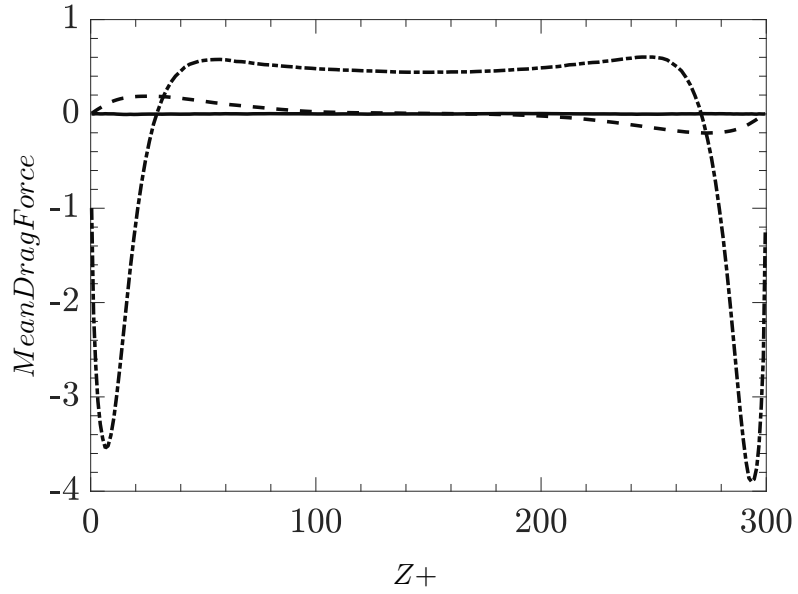

Figure 5.7: Directional components of drag force acting from the fluid on the particles in case NH; Figure legends : (——) spanwise, (– –) wall-normal, (–·–) streamwise

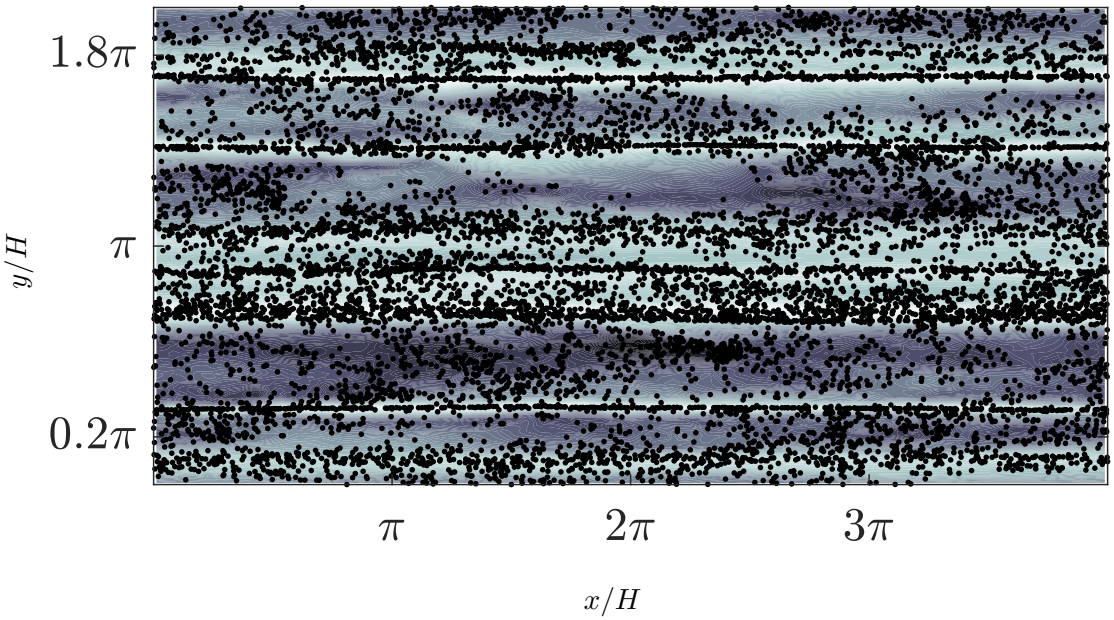

Figure 5.8: Instantaneous contours of mean streamwise velocity with particles in wall-normal plane near the wall for case NH

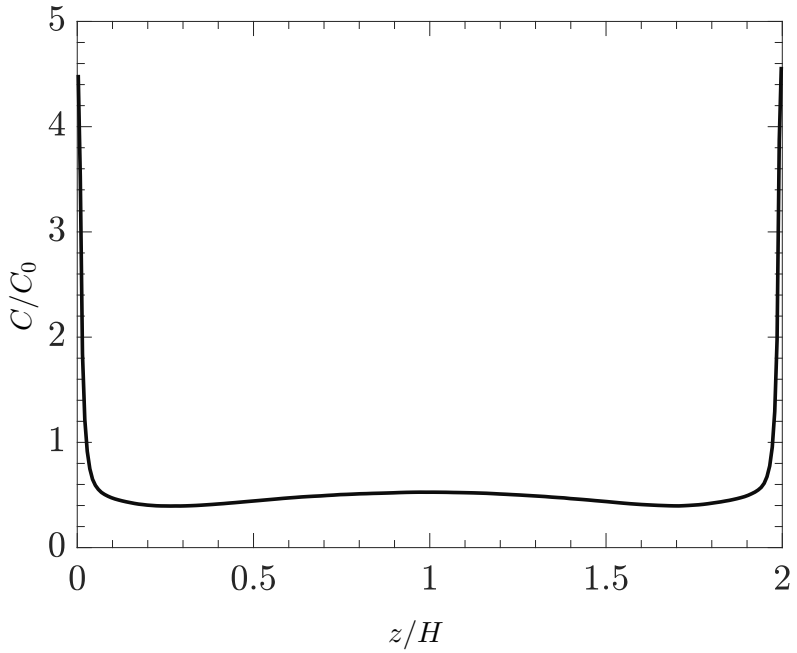

Figure 5.9: Particle concentration in the channel as a function of wall-normal distance in case NH

fluid velocities and hence particles exert work on to the fluid. In the core region, the drag is positive that means the fluid exerts work on to the particles. Thus the particles receive energy from the core region and return most of it in the near wall regions, with some dissipation as reported by Zhao et al. [21]. Thus, kinetic energy is drained from the fluid-particle system by means of particle dissipation. This particle dissipation is however insufficient to dampen the streamwise velocity fluctuations, which slightly increase in the near wall region due to work done by particles on the local fluid. However, this dissipation is responsible for drastic reduction in spanwise and wall-normal components of velocity fluctuations and Reynolds stress indicating overall decay of turbulence in fluid-particle suspensions as shown in figure 5.6. For a more detailed analysis, the reader is reffered to the work of Zhao et al. [21]

5.4 Thermal behaviour

The focus of this thesis is on the thermal behaviour of fluid in the presence of particles. First the contour plots of instantaneous temperature and velocity field near the walls is presented. Then the changes in mean temperature and heat transfer modes are presented. Later on the temperature variance and budgets of temperature variance are presented to further analyze the possible mechanisms that alter the thermal field in a particle-laden channel flow.

5.4.1 Instantaneous contours of mean temperature and mean streamwise velocity

In chapter (2), behaviour of momentum and energy transfer was discussed. As can be seen from equation (2.6) and equation (2.7), both these quantities are transported due to advection and diffusion. Both equations are quite similar in nature. The difference in nature of source term in two phenomena will result in difference in momentum and thermal behaviour. Since the energy source term in dependent on local streamwise velocity, a correlation between local streamwise velocity and local temperature is expected. This can be also be seen in figure 5.10 and figure 5.11. It is also noted from figure 5.10 and figure 5.11 that higher streamwise velocities correspond to higher temperatures near the hot wall while the low speed streaks are associated with lower temperatures near the cold wall. This is because there is strong negative correlation between streamwise velocity fluctuations and temperature fluctuations in heated region and strong positive correlation in the cold region (figure 5.12).

5.4.2 Mean Properties

Figure 5.13 shows the mean temperature ($\overline{\theta}$) profiles for different cases as a function of wall-normal coordinate. It can be seen that the temperature distribution is greatly affected by the particle Stokes number and thermal Stokes number. A comparison of temperature profile for case NP and case NH shows that there is an increased heat transfer due to the presence of particles. It can also be noted that as the optical thickness of the fluid is increased, particles absorb more heat which penetrate deeper in the channel (as the

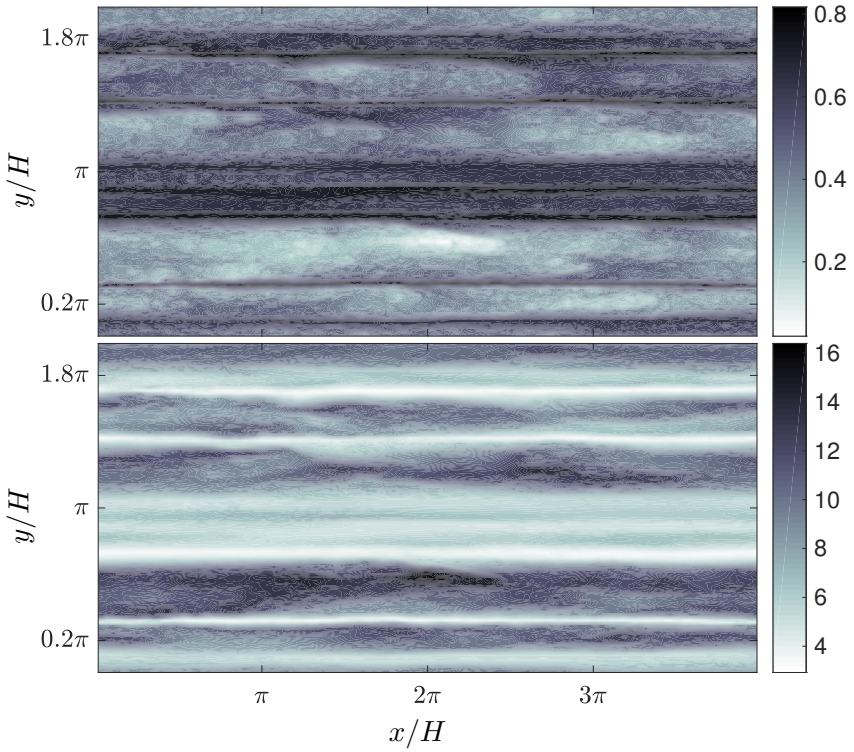

Figure 5.10: Instantaneous contours of mean properties near hot wall a) Streamwise Velocity

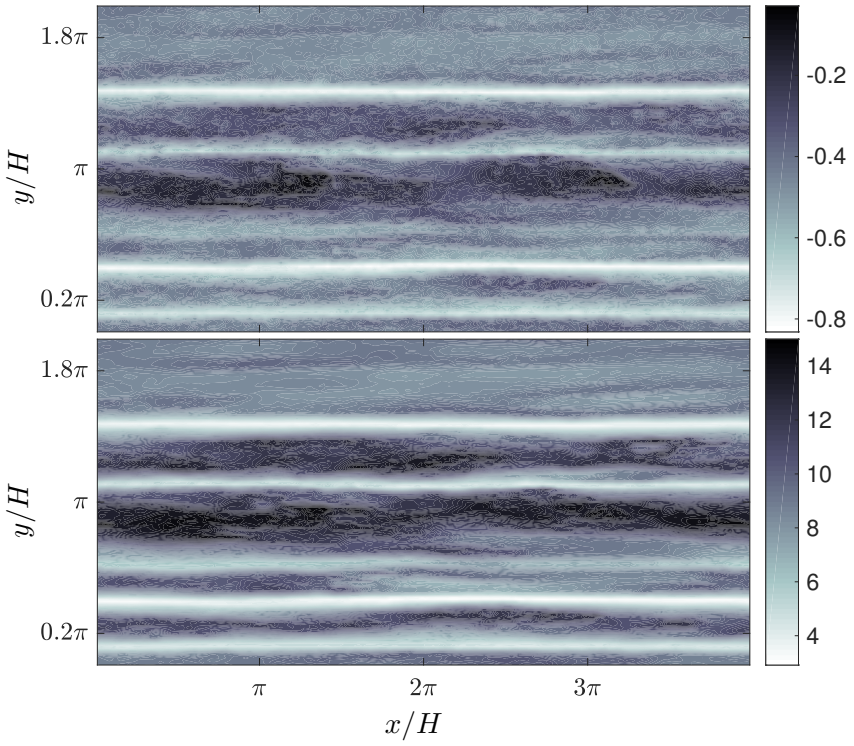

Figure 5.11: Instantaneous contours of mean properties near cold wall a) Streamwise Velocity b) Temperature

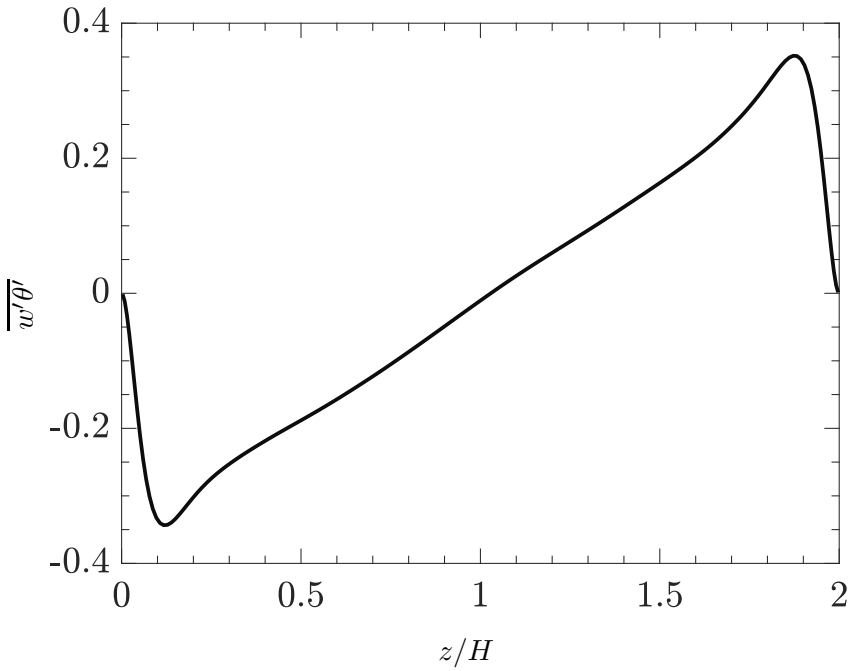

Figure 5.12: Correlation of streamwise velocity and temperature fluctuations as a function of wall-normal distance for case NH

length scales of radiative heat transfer reduce). As a result, there is an overall increase of mean temperature in the flow. Also from the comparison of mean temperature profile for case OT5 and St50, it can be seen that as the particle thermal Stokes number is reduced, heat transfer is also reduced and there is a higher temperature in the core of the channel. The reduced heat transfer is more prominent near the hotter wall.

5.4.3 Heat Flux

Heat fluxes are derived from the averaged energy equation. For clarity, it is rewritten here:

$$\frac{\partial}{\partial z}\left(\frac{1}{Re_\tau Pr}\frac{\partial\overline{\theta}}{\partial z} - \overline{u'\theta'}\right) + \overline{q_{2w}} = 0. \tag{5.7}$$

Integrating equation (5.7) in wall-normal direction (z) yields:

$$\frac{1}{Re_\tau Pr}\frac{\partial\overline{\theta}}{\partial z} - \overline{u'\theta'} + \int_0^z \overline{q_{2w}}dz = C_1, \tag{5.8}$$

where, C_1 is an integration constant. The three terms on the LHS of equation (5.8) represent the three heat transfer modes defined as:

$$\bar{q}_{mol} = \frac{1}{Re_\tau Pr}\frac{\partial\overline{\theta}}{\partial z}, \quad \bar{q}_{turb} = -\overline{u'\theta'}, \quad \bar{q}_{part} = \int_0^z \overline{q_{2w}}dz \tag{5.9}$$

where, $\bar{q}_{mol}$ is the molecular heat flux, $\bar{q}_{turb}$ is the turbulent heat flux and $\bar{q}_{part}$ is the particle feedback heat flux.

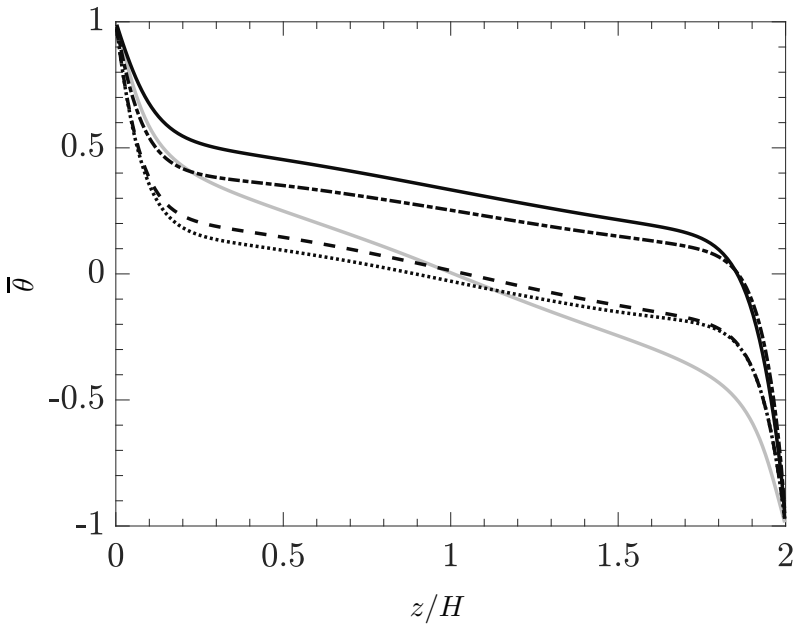

Figure 5.13: Comparison of Mean Temperature Profiles; Figure legends : (——) reference case, (·····) case NH, (– –) case OT01, (–·–) case OT5, (——) case St50

Figure 5.14 shows the heat transfer mechanisms in present simulations. Figure 5.14(a) shows the overall heat transfer in the channel. It can be seen that the overall heat transfer remains constant in the core of the channel. However, it is not constant near the wall. This may be because the particle streaks are much longer and not uncorrelated for the chosen domain length, but still it gives an insight into the heat transfer mechanisms for the different cases. Figures 5.14(b) to 5.14(d) show the contribution of three different mechanisms as described in equation (5.9). From figure 5.14(a), a considerable increase in overall heat flux is noticed for cases NH,OT01 and OT05, while there is reduction in overall heat flux for case St50. Also, it can be seen that the heat flux is reduced with increased optical thickness. It is noted from figure 5.14(c) and 5.14(d) that turbulent heat transfer and molecular heat transfer is drastically reduced in the presence of particles, especially in the core of the channel. This is because the particles decay the turbulence in the channel and hence the turbulent heat transfer is reduced. The molecular heat transfer is reduced in the centre of the channel because the gradient of mean temperature is reduced in the presence of particles as an be seen in from figure 5.13. From figure 5.14, it is clear that the particle feedback heat flux is the dominating mode of heat transfer. The particle feedback heat flux decreases with increasing optical thickness of the fluid and hence the overall heat transfer is also reduced. With reduction in thermal Stokes number, the heat carrying capacity of particles is reduced due to smaller thermal response time and hence the mixing of heat in the channel is inhibited drastically reducing the contribution of particle heat flux. As a result, the total heat flux in this case is even lower than the reference case with no particles. This is because the increase of heat transfer that is associated with particle feedback heat flux is dominated by the reduction of turbulent and molecular heat transfer. Also it can be seen that in case of external sources (case OT01, case OT5 and St50), there is a reversal in the direction of particle heat flux in the vicinity of cold wall from where the external heat is incident on the particles. In this region, heat

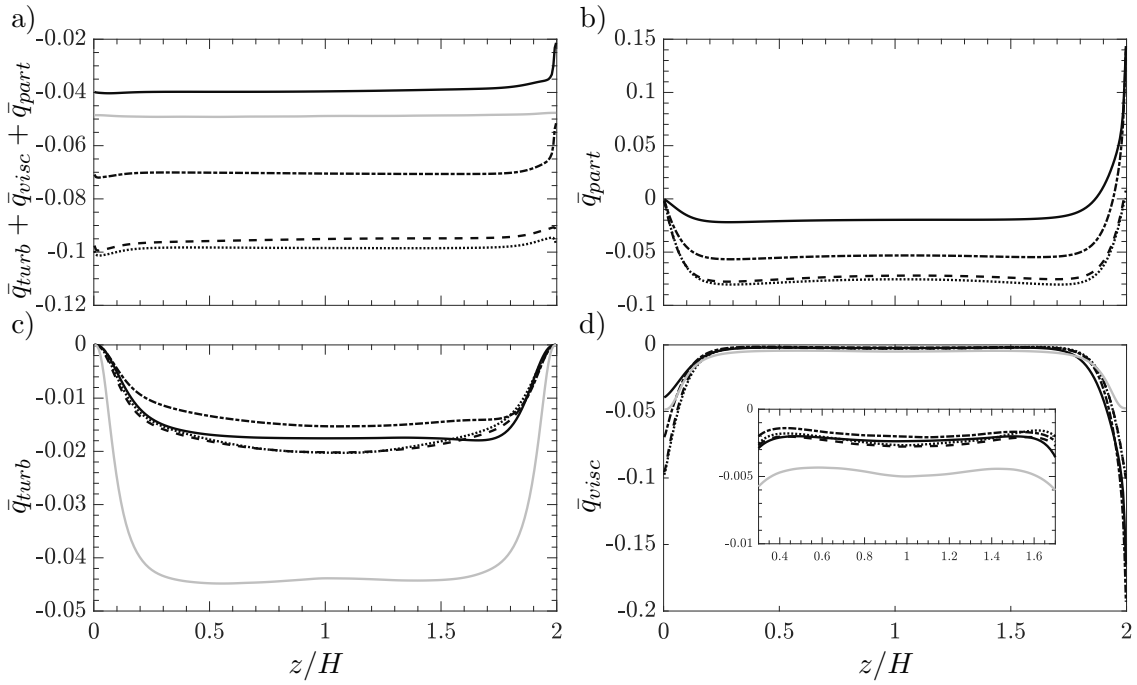

Figure 5.14: Heat transfer mechanisms. (a): total heat flux; (b): mean particle heat flux; (c): mean wall normal turbulent heat flux; (d): mean viscous heat flux; Figure legends : (——) reference case, (·····) case NH, (– –) case OT01, (–·–) case OT5, (——) case St50

flux is positive, that means particle receive heat from external source, thereby increasing the overall temperature of the fluid-particle system. This is responsible for higher mean temperature profiles for external heat cases as seen in figure 5.13. For smaller thermal Stokes number, particles retain less heat within themselves and release more heat into the fluid, which is reflected in higher temperatures for case St50 than in case OT5.

5.4.4 Temperature variance and budgets of temperature variance

Temperature variance

In this section, modulation of temperature fluctuations in the presence of particles will be discussed. The temperature variance for the present simulations are shown in figure 5.15. It can be seen that with the presence of particles, the temperature variance near the wall increases with the presence of particles, while it reduces in the core of the channel (compare reference case with case NH). It can also be seen that as the optical thickness of the fluid increases, the temperature variance is reduced, especially near the hot wall (compare case OT01 and case OT5). Also, the absorption of energy by particles in an optically thick medium breaks down the symmetry of the temperature variance as evident from case OT5 and case St50. The temperature variance can be analyzed in more detail from the equation of temperature fluctuations:

$$\frac{\partial \theta'}{\partial t} + \frac{\partial \bar{u}_j \theta'}{\partial x_j} + \frac{\partial u'_j \bar{\theta}}{\partial x_j} + \frac{\partial u'_j \theta'}{\partial x_j} - \frac{\partial \overline{u'_j \theta'}}{\partial x_j} = \frac{1}{Re_\tau Pr} \frac{\partial^2 \theta'}{\partial x_j^2} + q'_{2w}. \tag{5.10}$$

The budget equation for temperature variance can be derived by multiplying equation (5.10) with θ' and applying reynolds averaging. The resulting equation becomes:

$$0 = -2\overline{w'\theta'}\frac{\partial\bar{\theta}}{\partial z} + \frac{\partial}{\partial z}\left(\frac{1}{Re_\tau Pr}\frac{\partial\overline{\theta'^2}}{\partial z} - \overline{w'\theta'^2}\right) - \frac{2}{Re_\tau Pr}\overline{\left(\frac{\partial\theta'}{\partial x_j}\right)^2} + \overline{\theta' q'_{2w}}. \tag{5.11}$$

Individual description of the terms is written below:

- Turbulent Production, $\mathcal{P}_\theta = -2\overline{w'\theta'}\frac{\partial\bar{\theta}}{\partial z}$
- Turbulent Transport, $\mathcal{T}_\theta = \frac{\partial}{\partial z}\left(\overline{w'\theta'^2}\right)$
- Molecular diffusion, $\phi_m = \frac{1}{Re_\tau Pr}\frac{\partial^2\overline{\theta'^2}}{\partial z^2}$
- Molecular dissipation, $\epsilon_m = -\frac{2}{Re_\tau Pr}\overline{\left(\frac{\partial\theta'}{\partial x_j}\right)^2}$
- Particle term $\mathcal{Q}_{part} = \overline{\theta' q'_{2w}}$

q'_{2w} is always positively correlated with temperature fluctuations θ' as can be seen in figure 5.16. Therefore the particle term, $\overline{\theta' q'_{2w}}$ acts as the source term for the temperature fluctuations. From the figure 5.16 it is evident that as the optical thickness is increased, the source term q'_{2w} reduces. As a result, temperature variance is also reduced. The asymmetry in this term leads to asymmetry in the temperature variance.

However, the reduction in temperature fluctuations in the presence of particles is not attributed to this term, since this term is negligible in the core of the channel. The main reason of the decrease and flattening out of the temperature variance in the centre of the channel is the reduction in the magnitude of wall normal fluctuations w', which reduce the production and turbulent transport term in the temperature variance budget.

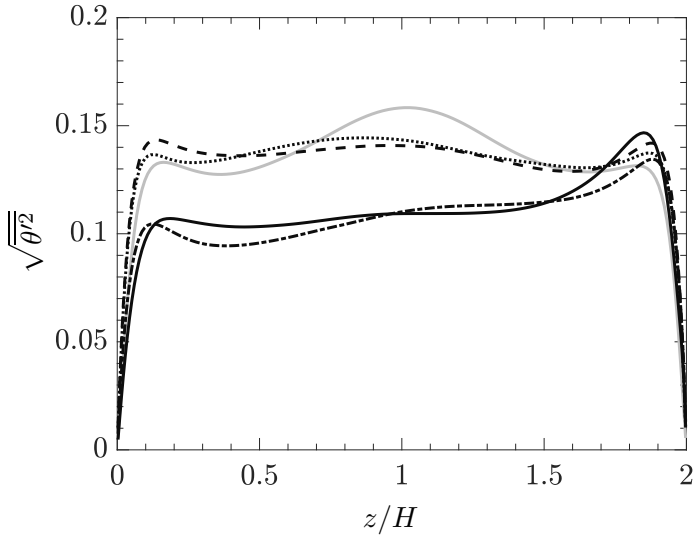

Figure 5.15: Comparison of turbulent intensity of temperature fluctuations; Figure legends : (——) reference case, (·····) case NH, (– –) case OT01, (–·–) case OT5, (——) case St50

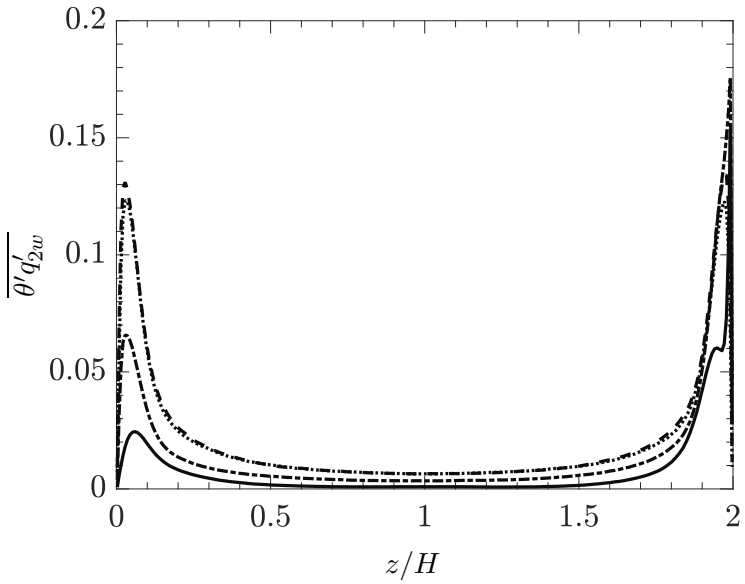

Figure 5.16: Particle term $\mathcal{Q}_{part}$ for different cases; Figure legends : (·····) case NH, (– –) case OT01, (–·–) case OT5, (——) case St50

Budgets of temperature variance

The budget equation for temperature variance is discussed next to highlight the effect of different phenomena on temperature fluctuations. The complete budget equation is written in equation (5.11). Figure 5.17 reports the budgets of temperature variance for the reference case with no particles. Due to the symmetry of temperature profile, the profiles for different budget terms are also symmetric. Close to the wall, in the viscous sublayer, molecular diffusion dominates, with molecular diffusion being balanced by molecular dissipation. The production term peaks near the walls. This is because of the high temperature gradient of the mean temperature, which ensures high production rate of temperature variance. In the core of the channel, production term is balanced by the molecular dissipation term. The turbulent transport term neither creates or destroys the temperature fluctuations, it simply redistributes the fluctuations towards the wall and towards the centre of the channel.

Figure 5.18 presents the budgets for the case NH, for particles without any external heating. The profiles of the budgets are still symmetrical, since there is no dissimilar heating of the particles, and the mean temperature profile remain symmetric. Due to presence of particles near the wall, the turbulence is decayed and hence the production term is also reduced in magnitude. However in the viscous sublayer, molecular effects increase and a high molecular diffusion is seen in this case. It should be noted that there is another source term for temperature fluctuations, $\mathcal{Q}_{part}$, which acts in a similar way as the production term. To balance the increased molecular diffusion and particle term, molecular dissipation is enhanced near the walls. In the core of the channel, the turbulence is already decayed and the particle concentration is also reduced. As a result, we see lower dissipation term balancing the lower production and particle term.

Figure 5.19 shows the budgets for the case OT01. The profiles of the temperature variance budget start to get asymmetrical, with slightly higher molecular dissipation and particle

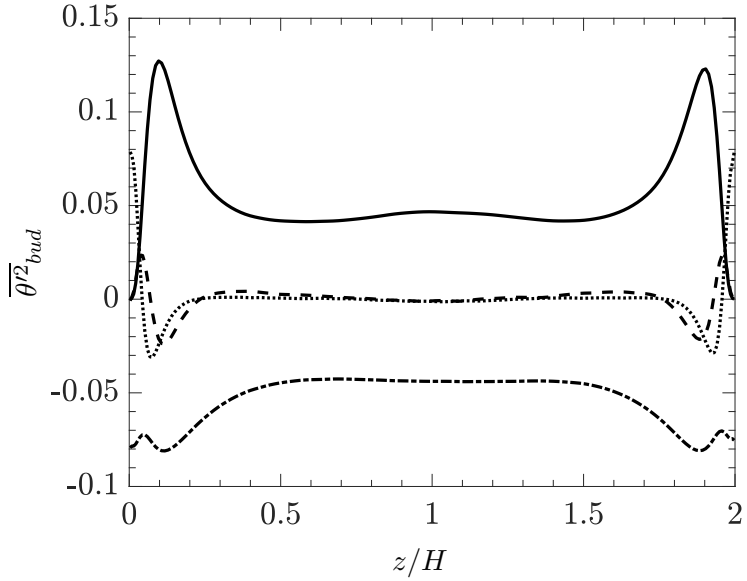

Figure 5.17: Budgets of temperature variance for Reference case; Figure legends : (·····) molecular diffusion, (– –) turbulent transport, (–·–) dissipation, (——) production

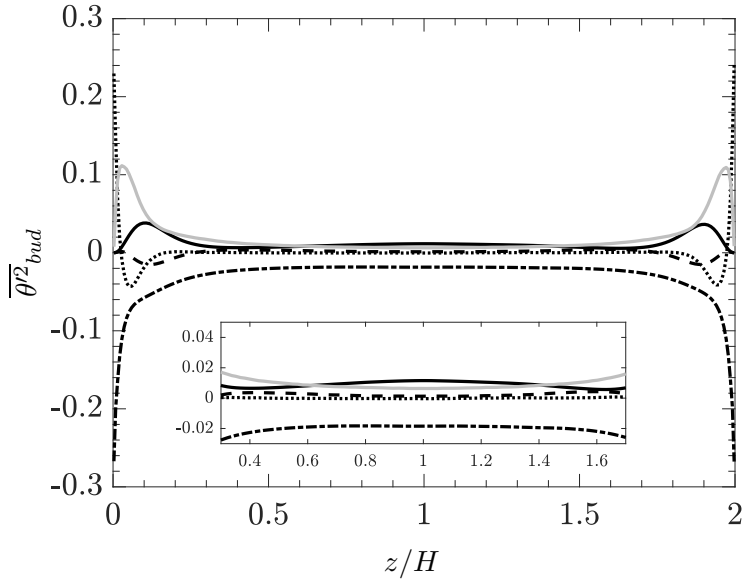

Figure 5.18: Budgets of temperature variance for case NH; Figure legends : (·····) molecular diffusion, (– –) turbulent transport, (–·–) dissipation, (——) production, (——) particle term

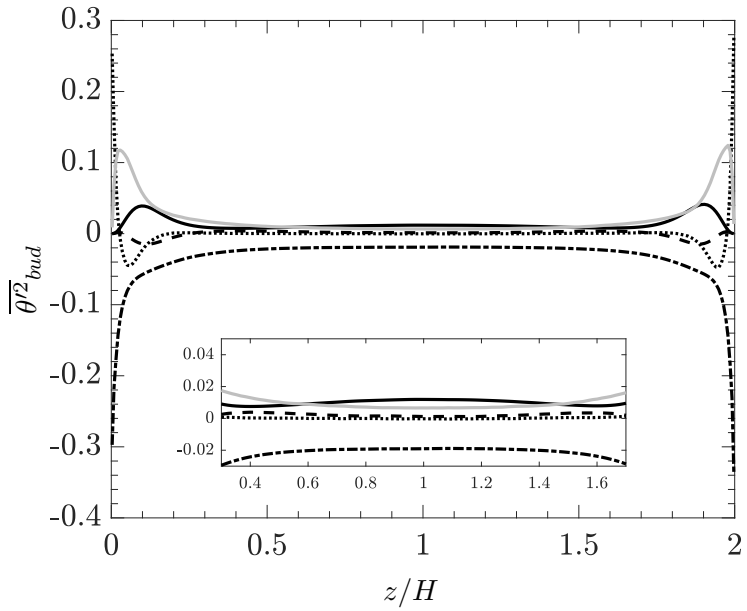

Figure 5.19: Budgets of temperature variance for case OT01; Figure legends : (·····) molecular diffusion, (– –) turbulent transport, (–·–) dissipation, (——) production, (——) particle term

term near the cold wall. This increase in particle term is only slightly higher than for the particle term in case NH, as such there is a slight increase in temperature fluctuations near the walls.

Figure 5.20 presents the budgets for the case OT5. In this case, highly asymmetrical profiles can be seen in the temperature budget due to asymmetry in temperature fluctuations and mean temperature. In this case, the production term reduces near the hot wall due to decrease in wall normal fluctuations, w'. The production term, however, remains nearly the same near the cold wall. This is because the increase in mean temperature gradient is offset by decrease in wall-normal velocity fluctuations, w'. The particle term also follows the same trend and decreases near the hot wall and increases near the cold wall. This is because, heat is added near the cold wall resulting in higher temperature variations. Near the hot wall, the temperature fluctuations reduce since the heat is transferred to hot wall from a higher temperature than in case NH or case OT01. As a result, to balance the production and particle term, molecular dissipation also follow the same trend. It reduces near the hot wall and increases near the cold wall. A similar behaviour is seen for molecular dissipation as well.

Figure 5.21 reports the budgets for case St50. The reduction in $\mathcal{Q}_{part}$ is because of the smaller thermal Stokes number, which reduces the heat carrying capacity of the particles and hence reduces the feedback flux from particle to fluid resulting in lower values of q'_{2w}. The production term is only slightly higher for the case St50 than case OT5. This is because of slightly higher gradient of mean temperature as shown in figure 5.13. The dissipation term also reduce only near the wall to balance the production and particle term. In the core of the channel, the total increase in production term and particle term is almost same for both the cases St50 and OT5, thus there is no difference in dissipation term in the core of the channel. As such there is only nominal difference in the fluctuations

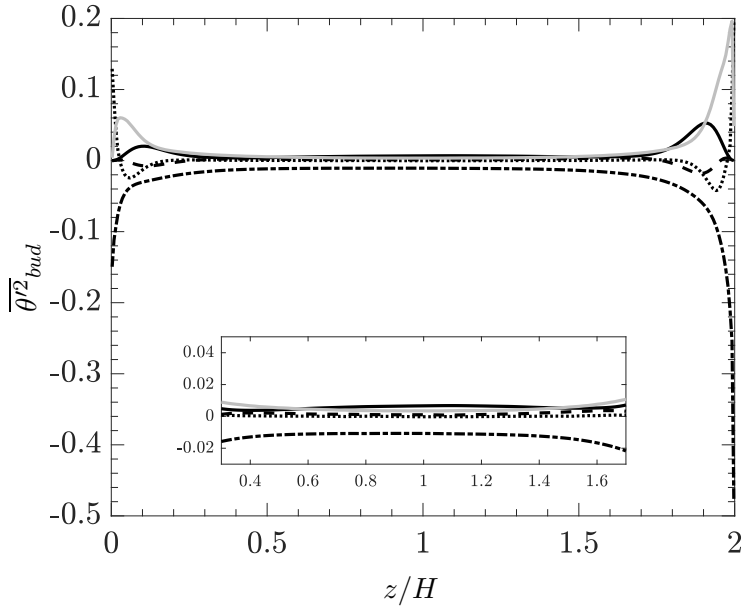

Figure 5.20: Budgets of temperature variance for case OT5; Figure legends : (·····) molecular diffusion, (– –) turbulent transport, (–·–) dissipation, (——) production, (——) particle term

in case St50 and case OT5.

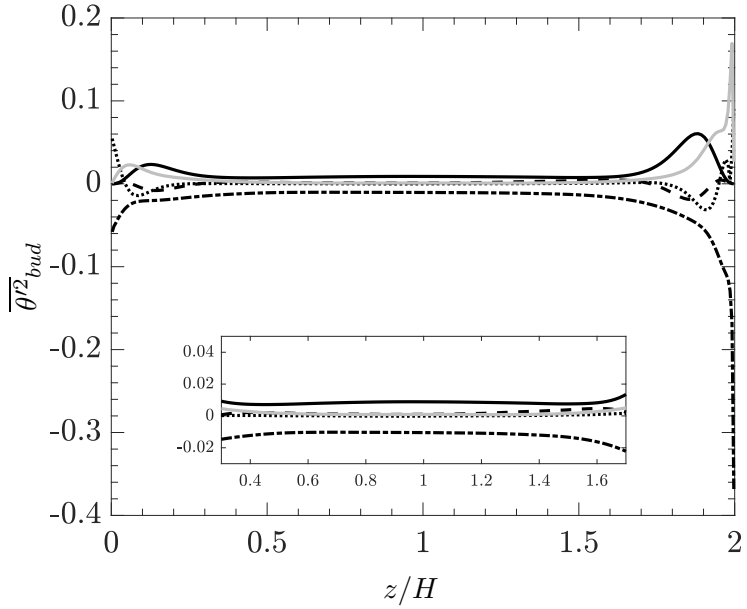

Figure 5.21: Budgets of temperature variance for case St50; Figure legends : (·····) molecular diffusion, (– –) turbulent transport, (–·–) dissipation, (——) production, (——) particle term

Chapter 6

Conclusions and Recommendations

6.1 Conclusions

In the present work, a comprehensive study of heat transfer in particle-laden turbulent channel flow has been performed. The modification of temperature field in the presence of particles which receive heat from an external radiation source in an optically thick medium is extensively investigated. This is done with the aid of mean temperature profiles, temperature variance and budgets of temperature variance.

In order to carry out the study the heat transfer in particle-laden turbulent channel flow, the existing DNS code developed by Boersma [5] has been modified to include particle transport. The point-particle approach with two way coupling is implemented using trilinear interpolation scheme and 3^{rd} order Runge-Kutta time marching scheme. The developed code is validated using the results from Kuerten et al.[20]. Using this code, four cases different cases have been investigated. The four cases encompass, no external heating of particles and three different optical thickness for the fluid.

The particles, in general, tend to increase the heat transfer in the turbulent channel flow. However for some cases, the presence of particles can result in decrease in overall heat transfer. This happens when the particle thermal Stokes number is so low (case St50) that the increased heat transfer due to particles is dominated by the reduction in heat transfer due to decay in turbulence. The dominating mechanism for the heat transfer in particle-laden flows is the particle feedback heat flux. The particles absorb heat from hotter regions and release this heat when they move to colder regions, thereby enhancing the overall heat transfer.

Furthermore, a study of temperature variance and budgets of temperature variance, further highlights the role of this particle feedback heat flux in the modification of temperature field. In the presence of particles, the production term reduces, while the particle feedback term increases the thermal turbulence drastically. This effect is enhanced at higher optical thickness of the fluid and ultimately breaks down the symmetry of the temperature field.

It can therefore be concluded that particles, optical thickness of the fluid and external heating of particles play an important role in modifying the temperature field in a turbulent channel flow.

6.2 Recommendations

This work provides a general framework to study particle-laden turbulent channel flow. The developed particle module is implemented in such a manner that it can be easily used for other flow geometries as well. The limitation of the trilinear interpolation scheme is that it is applicable only to a cartesian grid. This can be made general by using Lagrangian or cubic spline interpolation schemes. If a more accurate description is required, it is recommended to use a much bigger domain length such that the particle streaks become completely uncorrelated. Furthermore this analysis could be done using a radiation solver to be more accurate. Finally, this analysis could also be extended to compressible fluids, thereby moving closer to real world.

References

[1] P. Bagchi and S. Balachandar. Effect of turbulence on the drag and lift of a particle. *Physics of Fluids*, 15(11):3496–3513, 2003.

[2] S. Balachandar. A scaling analysis for point-particle approaches to turbulent multiphase flows, 2009.

[3] S. Balachandar and John K. Eaton. Turbulent Dispersed Multiphase Flow. *Annual Review of Fluid Mechanics*, 42(1):111–133, 2010.

[4] G. K. Batchelor. Small-scale variation of convected quantities like temperature in turbulent fluid Part 1. General discussion and the case of small conductivity. *Journal of Fluid Mechanics*, 5(01):113, jan 1959.

[5] Bendiks Jan Boersma. A 6th order staggered compact finite difference method for the incompressible Navier-Stokes and scalar transport equations. *Journal of Computational Physics*, 230(12):4940–4954, 2011.

[6] Marc Boivin, Olivier Simonin, and Kyle D. Squires. Direct numerical simulation of turbulence modulation by particles in isotropic turbulence. *Journal of Fluid Mechanics*, 375:235–263, 1998.

[7] Tristan M. Burton and John K. Eaton. Fully resolved simulations of particle-turbulence interaction. *Journal of Fluid Mechanics*, 545(-1):67, 2005.

[8] Andreas Ten Cate, Jos J. Derksen, Luis M. Portela, and Harry E. A. Van Den Akker. Fully resolved simulations of colliding monodisperse spheres in forced isotropic turbulence. *Journal of Fluid Mechanics*, 519:233–271, 2004.

[9] Clayton T Crowe, Martin Sommerfeld, and Yutaka Tsuji. *Multiphase Flows with Droplets and Particles*. 1998.

[10] J. K. Eaton and J. R. Fessler. Preferential concentration of particles by turbulence. *International Journal of Multiphase Flow*, 20(SUPPL. 1):169–209, 1994.

[11] S. Elghobashi. Particle-laden turbulent flows: direct simulation and closure models. *Applied Scientific Research*, 48(3-4):301–314, 1991.

[12] S. Elghobashi. On predicting particle-laden turbulent flows. *Applied Scientific Research*, 52(4):309–329, 1994.

[13] Pierre Février, Olivier Simonin, and Kyle D. Squires. Partitioning of particle velocities in gassolid turbulent flows into a continuous field and a spatially uncorrelated random distribution: theoretical formalism and numerical study. *Journal of Fluid Mechanics*, 533:1–46, jun 2005.

[14] C. William Gear. *Numerical Initial Value Problems in Ordinary Differential Equations*. Prentice Hall PTR, Upper Saddle River, NJ, USA, 1971.

[15] Holger Homann and Jérémie Bec. Finite-size effects in the dynamics of neutrally buoyant particles in turbulent flow. *Journal of Fluid Mechanics*, 651:81, 2010.

[16] M Jaszczur. Numerical analysis of a fully developed non-isothermal particle-laden turbulent channel flow. *Archives of Mechanics*, 63(1):77–91, 2011.

[17] Nobuhide Kasagi. Progress in direct numerical simulation of turbulent transport and its control. *International Journal of Heat and Fluid Flow*, 19(2):125–134, 1998.

[18] J Kim, P Moin, and R Moser. Turbulence statistics in fully developed channel flow at low Reynolds number. *Journal of Fluid Mechanics*, 177(220):133–166, 1987.

[19] Donald L. Koch. Kinetic theory for a monodisperse gassolid suspension. *Physics of Fluids A: Fluid Dynamics*, 2(10):1711, 1990.

[20] J. G M Kuerten, C. W M van der Geld, and B. J. Geurts. Turbulence modification and heat transfer enhancement by inertial particles in turbulent channel flow. *Physics of Fluids*, 23(12), 2011.

[21] Zhao Lihao, Helge I. Andersson, Jurriaan J. J. Gillissen, and Lihao Zhao. Interphasial energy transfer and particle dissipation in particle-laden wall turbulence. *Journal of Fluid Mechanics*, 715:32–59, 2013.

[22] S. L. Lyons, T. J. Hanratty, and J. B. McLaughlin. Direct numerical simulation of passive heat transfer in a turbulent channel flow. *International Journal of Heat and Mass Transfer*, 34(4-5):1149–1161, 1991.

[23] J. G. M. Kuerten. Point-Particle DNS and LES of Particle-Laden Turbulent flow - a state-of-the-art review, 2016.

[24] C. Marchioli, A. Soldati, J. G M Kuerten, B. Arcen, A. Tanière, G. Goldensoph, K. D. Squires, M. F. Cargnelutti, and L. M. Portela. Statistics of particle dispersion in direct numerical simulations of wall-bounded turbulence: Results of an international collaborative benchmark test. *International Journal of Multiphase Flow*, 34(9):879–893, 2008.

[25] M R Maxey, B K Patel, E J Chang, and L-P Wang. Simulations of dispersed turbulent multiphase flow. *Fluid Dynamics Research*, 20(1-6):143–156, 1997.

[26] Maxey Martin R. The gravitational settling of aerosol particles in homogeneous turbulence and random flow fields. *Journal of Fluid Mechanics*, 174(1987):441–465, 1987.

[27] E. E. Michaelides. ReviewThe Transient Equation of Motion for Particles, Bubbles, and Droplets. *Journal of Fluids Engineering*, 119(2):233, 1997.

[28] Frans T.M. Nieuwstadt, Jerry Westerweel, and Bendiks J. Boersma. *Turbulence: Introduction to Theory and Applications of Turbulent Flows*. Springer, 1st ed. 2016 edition, 7 2016.

[29] Francesco Picano, Wim-Paul Breugem, and Luca Brandt. Turbulent channel flow of dense suspensions of neutrally buoyant spheres. *Journal of Fluid Mechanics*, 764:463–487, 2015.

[30] Stephen B. Pope. *Turbulent Flows*, volume 1. 2000.

[31] L M Portela and R V A Oliemans. *Direct and Large-Eddy Simulation of Particle-Laden Flows Using the Point-Particle Approach*, pages 453–460. Springer Netherlands, Dordrecht, 2001.

[32] Luís M. Portela and René V.A. Oliemans. Eulerian-Lagrangian DNS/LES of particle-turbulence interactions in wall-bounded flows. *International Journal for Numerical Methods in Fluids*, 43(9):1045–1065, 2003.

[33] H. Pouransari, H. Kolla, J. H. Chen, and A. Mani. Spectral analysis of energy transfer in turbulent flows laden with heated particles. *Journal of Fluid Mechanics*, 813:1156–1175, 2017.

[34] L Prandtl. Bericht über Untersuchungen zur ausgebildeten Turbulenz. *Zeitschrift fur angewandte Mathematik und Mechanik*, 5(1925):136 – 139, 1925.

[35] W. E. Ranz and W. R. Marshall. Evaporation from drops - Part 1, 1952.

[36] O. Reynolds. An Experimental Investigation of the Circumstances Which Determine Whether the Motion of Water Shall Be Direct or Sinuous, and of the Law of Resistance in Parallel Channels. *Philosophical Transactions of the Royal Society of London*, 174(0):935–982, 1883.

[37] Lewis Fry Richardson. *Weather Prediction by Numerical Process*. 1922.

[38] Salvatore J. Rossetti and Robert Pfeffer. Drag reduction in dilute flowing gassolid suspensions. *AIChE Journal*, 18(1):31–39, 1972.

[39] P. G. Saffman. On the Settling Speed of Free and Fixed Suspensions. *Studies in Applied Mathematics*, 52(2):115–127, jun 1973.

[40] L. Schiller and Z. Naumann. A drag coefficient correlation. *Z.Ver.Deutsch.Ing*, 77(13-14):318–320, 1933.

[41] Shao-lee Soo. *Multiphase fluid dynamics*. Gower Technical Press, 1990.

[42] Kyle D. Squires and John K. Eaton. Particle response and turbulence modification in isotropic turbulence. *Physics of Fluids A: Fluid Dynamics*, 2(7):1191–1203, 1990.

[43] Kyle D. Squires and John K. Eaton. Preferential concentration of particles by turbulence. *Physics of fluids. A, Fluid dynamics*, 3(5):1169–1178, 1991.

[44] Shivshankar Sundaram and Lance R. Collins. Collision statistics in an isotropic particle-laden turbulent suspension. Part 1. Direct numerical simulations. *Journal of Fluid Mechanics*, 335:75–109, 1997.

[45] Markus Uhlmann. An immersed boundary method with direct forcing for the simulation of particulate flows. *Journal of Computational Physics*, 209(2):448–476, 2005.

[46] Romboud van de Woestijne. Direct Numerical Simulation of Particle-Laden Turbulent Channel Flow with Heat Transfer . Master's thesis, Delft University of Technology, The Netherlands, 2013.

[47] Bas van Haarlem, Bendiks J Boersma, and Frans TM Nieuwstadt. Direct numerical simulation of particle deposition onto a free-slip and no-slip surface. *Physics of Fluids*, 10(10):2608–2620, 1998.

[48] A. W. Vreman. Turbulence characteristics of particle-laden pipe flow. *Journal of Fluid Mechanics*, 584:235, aug 2007.

[49] A. W. Vreman. Particle-resolved direct numerical simulation of homogeneous isotropic turbulence modified by small fixed spheres. *Journal of Fluid Mechanics*, 796:40–85, 2016.

[50] F. Zhao, W. K. George, and Berend G M van Wachem. Four-way coupled simulations of small particles in turbulent channel flow: The effects of particle shape and Stokes number. *Physics of Fluids*, 27(8), 2015.

[51] F. Zonta, C. Marchioli, and Alfredo Soldati. Direct numerical simulation of turbulent heat transfer modulation in micro-dispersed channel flow. *Acta Mechanica*, 195(1-4):305–326, 2008.